

A Generalized Tensor Formulation for Hyperspectral Image Super-Resolution Under General Spatial Blurring

Yinjian Wang, Wei Li, *Senior Member, IEEE*, Yuanyuan Gui, Qian Du, *Fellow, IEEE*, and James E. Fowler, *Fellow, IEEE*

Abstract—Hyperspectral super-resolution is commonly accomplished by the fusing of a hyperspectral imaging of low spatial resolution with a multispectral image of high spatial resolution, and many tensor-based approaches to this task have been recently proposed. Yet, it is assumed in such tensor-based methods that the spatial-blurring operation that creates the observed hyperspectral image from the desired super-resolved image is separable into independent horizontal and vertical blurring. Recent work has argued that such separable spatial degradation is ill-equipped to model the operation of real sensors which may exhibit, for example, anisotropic blurring. To accommodate this fact, a generalized tensor formulation based on a Kronecker decomposition is proposed to handle any general spatial-degradation matrix, including those that are not separable as previously assumed. Analysis of the generalized formulation reveals conditions under which exact recovery of the desired super-resolved image is guaranteed, and a practical algorithm for such recovery, driven by a blockwise-group-sparsity regularization, is proposed. Extensive experimental results demonstrate that the proposed generalized tensor approach outperforms not only traditional matrix-based techniques but also state-of-the-art tensor-based methods; the gains with respect to the latter are especially significant in cases of anisotropic spatial blurring.

Index Terms—Image fusion, hyperspectral super-resolution, tensor factorization, recoverability, sparse coding, nonconvex surrogate.



1 INTRODUCTION

HYPERSPECTRAL imagery is designed to capture a densely-sampled spectral signature for each pixel in an image, providing much finer spectral information than other imaging modalities. However, limited by the trade-off in current optical imaging systems, detailed spectral information comes at the cost of low spatial resolution in a hyperspectral image (HSI) [1], [2]. This fact has severely restricted the use of HSI in such applications as classification, anomaly detection, and object tracking. To deal with this issue, HSI super-resolution (HSR) has been the subject of substantial recent work, and HSR can be most effectively achieved through the fusion of an HSI with an image possessing high spatial resolution, such as a multispectral image (MSI).

From the perspective of data reconstruction, HSR aims to recover the super-resolution HSI (SRI) from the observed HSI and MSI. Since the earliest HSR studies (e.g., [3], [4]), the spatial degradation from the SRI to the HSI, as well as the spectral degradation from the SRI to the MSI, are modeled in a manner of a matrix operation. In this article, we formally refer to such modeling as the matrix formulation of HSR

(i.e., MF-HSR). In the literature, MF-HSR is the most common framework for HSR, and it explicitly reflects the inherent ill-posedness of the HSR problem, since the degradation equations therein are undetermined. To alleviate such ill-posedness, much existing HSR work has taken into account various priors induced from the intrinsic spatial and spectral correlations of the SRI to develop MF-HSR methods through various means such as spectral unmixing [5], [6], [7], [8], [9], sparse/low-rank representation [10], [11], [12], [13], [14], [15], [16], [17], non-local similarities [18], Bayesian learning [19], [20], [21], [22], and deep learning [23], [24], [25].

Although MF-HSR fusion models can be effective, they all rely on the reshaping of the HSI into a 2D matrix, or 1D vector, for processing. However, there is increasing interest [18], [26], [27], [28] in instead considering the HSI as a 3D tensor in order to exploit higher-order characteristics. Accordingly, many efforts have been devoted to adopting tensor-analysis tools to build tensor-based HSR models (e.g., [28], [29], [30], [31], [32], [33], [34], [35]). To adequately exploit the low-dimensional structure of high-dimensional HSI data, the resulting tensor formulation of HSR (TF-HSR) usually performs factorization in every single dimension. Thus, the spatial domain is decomposed into two orthogonal dimensions which precludes the design of TF-based methods following the framework of MF-HSR, namely, the expressing of the spatial degradation as a single matrix operation. To address this problem, [26], [28] made the additional assumption that the spatial-degradation matrix is separable in the sense of being a Kronecker product of two independent vertical and horizontal degradation matrices. Using such Kronecker-separable spatial degradation, a multitude of TF-HSR methods (e.g., [28], [29], [30], [31],

- This paper is supported by the National Key R&D Program of China (Grant no. 2021YFB3900502). (Corresponding author: Wei Li.)
- Y. Wang, W. Li, and Y. Gui are with the School of Information and Electronics, Beijing Institute of Technology, and Beijing Key Laboratory of Fractional Signals and Systems, 100081 Beijing, China (e-mail: yinju@bit.edu.cn, liwei089@ieee.org, 953647315@qq.com).
- Q. Du and J. E. Fowler are with the Department of Electrical and Computer Engineering, Mississippi State University, Starkville, MS 39762 USA (e-mail: du@ece.msstate.edu, fowler@ece.msstate.edu).

[32], [33], [35], [36]) have appeared in recent literature and achieved state-of-the-art performance.

Yet, the success of a TF-HSR is highly dependent on the assumption of separability of the spatial-degradation matrix. As pointed out in [28], the separable assumption holds for the most commonly used average and Gaussian blurring kernels. However, it has been argued recently [37], [38], [39] that such a simple average kernel or isotropic Gaussian kernel (IGK) is insufficient to characterize blurring processes exhibited by real sensors. For HSI in particular, sensor motion may result in anisotropic blurring ill-captured by the usual IGK (e.g., [40], [41], [42]). In such cases, more general kernels, such as an anisotropic Gaussian kernel (AGK), may more accurately model real-world spatial blurring. Under this observation, several questions naturally arise. Does the separable assumption still hold under more realistic (anisotropic) blurring kernels? If it does not, is there a criterion according to which one can tell when TF-HSR is suitable, and when is not? And, for more realistic blurring kernels for which TF-HSR fails, what should be done to still take advantage of tensors in HSR?

In addition, another open issue for TF-HSR is blind HSR, i.e., in which HSR is conducted without knowledge of the spatial- and spectral-degradation matrices. MF-HSR models have achieved this goal by various techniques, since MF-HSR is based on the physical interpretation of the blurring process. However, such is not the case for TF-HSR models, wherein modeling of spatial blurring is mathematically-driven. As a result, it is not known how to best estimate the pair of matrices that constitute separable spatial blurring, and most TF-HSR techniques (e.g., [28], [30], [31], [32]) resort to simply entirely ignoring degradation information such that they remain agnostic to it.

In this paper, we examine the TF-HSR framework under the assumption of general blurring and determine that TF-HSR is not feasible under such conditions. Thus, we propose a generalization of the TF-HSR problem, which we refer to as generalized TF-HSR, or GTF-HSR. The conditions for exact recovery of the proposed GTF-HSR determined, and a two-stage optimization strategy is devised for iterative estimation under a block-sparsity prior. Specifically, the primary contributions of this paper are:

- We present GTF-HSR, which is based on the Kronecker decomposition. Leveraging the property of such decomposition, we obtain a generalized separable condition on the spatial-degradation matrix for GTF and establish an equivalency between the proposed GTF-HSR and MF-HSR. That is, the proposed GTF-HSR can be applied to as many cases as can MF-HSR, and, most importantly, when TF-HSR cannot.
- The proposed capacity of GTF-HSR to achieve exact SRI recovery (i.e., its *recoverability*) is analyzed, and the conditions for exact recovery are determined. We also deduce the conditions when exact recovery by TF-HSR is impossible, which further emphasizes the benefit of our generalized approach.
- We invoke a blockwise group sparsity (BGS) as a new, higher-level prior. The proposed BGS characterizes the grouped property of the sparsity in the core tensor of a Tucker decomposition of the SRI. With

the help of a tensor-unfolding strategy as well as a nonconvex surrogate, BGS is easily imposed upon the core tensor to regularize the GTF-HSR problem, managing to explore the multi-linear properties of higher-order data in a compact form in an algorithmic framework we call BGS-GTF-HSR.

- To tackle the resulting regularized large-scale nonconvex BGS-GTF-HSR optimization problem, a two-stage optimization strategy consisting of subspace identification and BGS coding is devised. In the first stage, we cascade the two spatial subspace bases extracted from the MSI and HSI through singular-value decomposition (SVD) and sparse-dictionary learning, estimating the spectral subspace from the HSI alone via SVD. In the second stage, the BGS coefficients are estimated by an alternating-directions optimization.
- Extensive experiments on both synthetic and real-world datasets for blind and non-blind HSR problems demonstrate the superiority of the proposed GTF-HSR method compared to not only traditional MF-HSR methods but also to state-of-the-art TF-HSR methods.

The remainder of the paper is organized as follows. First in Sec. 2, we overview requisite background on tensors as well as existing MF-HSR and TF-HSR frameworks. Then, in Sec. 3, we introduce GTF-HSR, analyze it and its recoverability, and compare it analytically to the TF-HSR strategy. Sec. 4 then introduces the BGS-GTF-HSR optimization algorithm, while Sec. 5 presents a body of experimental results. Finally, Sec. 6 concludes the manuscript.

2 BACKGROUND

In this section, we overview pertinent aspects of tensor mathematics and the Tucker decomposition, as well as formulations of HSR found in prior literature. Also, we briefly introduce AGK.

2.1 Tensors and Notation

In this paper, a scalar is denoted as a , a vector is denoted as \mathbf{a} , a matrix is denoted as \mathbf{A} , and an N -order tensor is denoted as \mathcal{A} . For two tensors \mathcal{A} and \mathcal{B} , we denote their inner product as $\langle \mathcal{A}, \mathcal{B} \rangle = \sum_{i_1, i_2, \dots, i_N} \mathcal{A}_{i_1, i_2, \dots, i_N} \mathcal{B}_{i_1, i_2, \dots, i_N}$ where $\mathcal{A}_{i_1, i_2, \dots, i_N}$ is the element at location (i_1, i_2, \dots, i_N) of \mathcal{A} . The Frobenius norm of a tensor is then defined by $\|\mathcal{A}\|_F = \sqrt{\langle \mathcal{A}, \mathcal{A} \rangle}$. The Kronecker product between matrices is denoted by \otimes , while $\text{col}\{\mathbf{A}\}$ and $\text{null}\{\mathbf{A}\}$ denote the column and null spaces of a matrix, respectively. If a variable is drawn from some absolutely continuous distribution, we call it “generic” after [43]. For an N -order tensor $\mathcal{A} \in \mathbb{R}^{I_1 \times I_2 \times \dots \times I_N}$, its mode- n unfolding is a matrix denoted by $\mathbf{A}_{[n]} \in \mathbb{R}^{I_n \times I_1 \dots I_{n-1} I_{n+1} \dots I_N}$. The mode- n product (denoted \times_n) between tensor $\mathcal{A} \in \mathbb{R}^{I_1 \times I_2 \times \dots \times I_N}$ and matrix $\mathbf{U} \in \mathbb{R}^{J \times I_n}$ is a tensor defined such that $(\mathcal{A} \times_n \mathbf{U})_{[n]} = \mathbf{U} \mathbf{A}_{[n]}$.

In the sequel, we use the notation $\text{reshape}(\cdot)$, $\text{permute}(\cdot)$, $\text{svd}(\cdot)$, and $\text{soft}(\cdot)$ to denote tensor operators with the corresponding functionality of their MATLAB namesakes. Accordingly, we define the vectorization and

unvectorization operators as $\text{Vec}(\cdot) = \text{reshape}(\cdot, [], 1)$ and $\text{Unv}(\cdot | J, K) = \text{reshape}(\cdot, J, K)$, respectively.

Finally, we define the Tucker decomposition of an arbitrary N -order tensor $\mathcal{Z} \in \mathbb{R}^{I_1 \times I_2 \times \dots \times I_N}$ as

$$\mathcal{Z} = \mathcal{G} \times_1 \mathbf{U}_1 \times_2 \mathbf{U}_2 \times_3 \dots \times_N \mathbf{U}_N, \quad (2.1)$$

where $\mathcal{G} \in \mathbb{R}^{J_1 \times J_2 \times \dots \times J_N}$ is the core tensor, and $\{\mathbf{U}_n \in \mathbb{R}^{I_n \times J_n}\}_{n=1}^N$ are the factor matrices. In line with this decomposition, the Tucker-rank of \mathcal{Z} is defined in a multi-rank form as

$$\text{rank}_T \{\mathcal{Z}\} = (\text{rank} \{\mathbf{Z}_{[1]}\}, \text{rank} \{\mathbf{Z}_{[2]}\}, \dots, \text{rank} \{\mathbf{Z}_{[N]}\}). \quad (2.2)$$

Note that Tucker decomposition exists if and only if $J_n \geq \text{rank} \{\mathbf{Z}_{[n]}\}, \forall n$. Two important calculation rules are

$$\mathbf{Z}_{[n]} = \mathbf{U}_n \mathbf{G}_{[n]} (\mathbf{U}_N \otimes \dots \otimes \mathbf{U}_{n+1} \otimes \mathbf{U}_{n-1} \otimes \dots \otimes \mathbf{U}_1)^T, \quad (2.3)$$

and

$$\text{Vec}(\mathcal{Z}) = (\mathbf{U}_N \otimes \dots \otimes \mathbf{U}_1) \text{Vec}(\mathcal{G}). \quad (2.4)$$

The reader is referred to, e.g., [44], for greater elaboration on the definitions and notations presented in this section.

2.2 Existing Formulations of HSR

We now describe mathematically the two main frameworks for HSR as existing in prior literature: MF-HSR and TF-HSR. These formulations are built on the assumption—common in the literature—of a spectral-degradation matrix \mathbf{R} that comprises a spectral-downsampling process, along with \mathbf{D} , a matrix that encapsulates the hyperspectral sensor's spatial blurring coupled with the subsampling entailed by the imaging process.

Definition 2.1 (MF-HSR). *Given HSI $\mathcal{X} \in \mathbb{R}^{m_1 \times m_2 \times S}$, MSI $\mathcal{Y} \in \mathbb{R}^{M_1 \times M_2 \times s}$, spectral-degradation matrix $\mathbf{R} \in \mathbb{R}^{s \times S}$, and spatial-degradation matrix $\mathbf{D} \in \mathbb{R}^{M_1 M_2 \times m_1 m_2}$, with $m_1 < M_1$, $m_2 < M_2$, and $s < S$, the MF-HSR problem seeks the most appropriate SRI $\mathcal{Z} \in \mathbb{R}^{M_1 \times M_2 \times S}$, such that*

$$\begin{aligned} \mathbf{X}_{[3]} &= \mathbf{Z}_{[3]} \mathbf{D}, \\ \mathbf{Y}_{[3]} &= \mathbf{R} \mathbf{Z}_{[3]}. \end{aligned} \quad (2.5)$$

Definition 2.2 (TF-HSR). *Given HSI $\mathcal{X} \in \mathbb{R}^{m_1 \times m_2 \times S}$, MSI $\mathcal{Y} \in \mathbb{R}^{M_1 \times M_2 \times s}$, spectral-degradation matrix $\mathbf{R} \in \mathbb{R}^{s \times S}$, and spatial-degradation matrices $\mathbf{P}_1 \in \mathbb{R}^{m_1 \times M_1}$ and $\mathbf{P}_2 \in \mathbb{R}^{m_2 \times M_2}$, with $m_1 < M_1$, $m_2 < M_2$, and $s < S$, the TF-HSR problem seeks the most appropriate SRI $\mathcal{Z} \in \mathbb{R}^{M_1 \times M_2 \times S}$, such that*

$$\begin{aligned} \mathcal{X} &= \mathcal{Z} \times_1 \mathbf{P}_1 \times_2 \mathbf{P}_2, \\ \mathcal{Y} &= \mathcal{Z} \times_3 \mathbf{R}. \end{aligned} \quad (2.6)$$

Additionally, TF-HSR implicitly requires a separable spatial-degradation operator:

Assumption 2.1. *Suppose $\mathbf{D} \in \mathbb{R}^{M_1 M_2 \times m_1 m_2}$ is the spatial-degradation matrix in MF-HSR, then TF-HSR assumes that there exist $\mathbf{P}_1 \in \mathbb{R}^{m_1 \times M_1}$ and $\mathbf{P}_2 \in \mathbb{R}^{m_2 \times M_2}$ such that*

$$\mathbf{D} = (\mathbf{P}_2 \otimes \mathbf{P}_1)^T. \quad (2.7)$$

2.3 AGK

Let $\Phi \in \mathbb{R}^{(2r+1) \times (2r+1)}$ denote an AGK. Then each of its elements, $\Phi_{i,j}$, is calculated as

$$\Phi_{i,j} = \frac{1}{2\pi} \sqrt{|\Lambda|} \exp\left(-\frac{1}{2}[i \ j] \Lambda [i \ j]^T\right), \quad (2.8)$$

$$i, j \in \{-r, \dots, r\}$$

where $\Lambda = \begin{bmatrix} \cos \theta & -\sin \theta \\ \sin \theta & \cos \theta \end{bmatrix} \begin{bmatrix} a \\ b \end{bmatrix} \begin{bmatrix} \cos \theta & \sin \theta \\ -\sin \theta & \cos \theta \end{bmatrix}$. Thus AGK is determined by three parameters θ, a, b . To guarantee the positive-definiteness of Λ , we require a, b to be positive. We also note that when $a = b$, AGK degrades to IGK.

3 A GENERALIZED TENSOR FORMULATION

To propose a generalized formulation for HSR that is more appropriate when spatial degradations are anisotropic, we first examine the feasibility of TF-HSR, specifically, the validity of Asm. 2.1. Then, in Sec. 3.2, we present the proposed GTF-HSR framework that generalizes TF-HSR in order to handle anisotropic degradation. We close this discussion with an examination of the potential of GTF-HSR to exactly recover the desired SRI as well as ramifications of blind HSR on this recovery in Secs. 3.3 and 3.4, respectively.

3.1 Feasibility of TF-HSR

To begin, we introduce the Kronecker decomposition (KD):

Theorem 3.1 (Kronecker Decomposition). *For any matrix $\mathbf{W} \in \mathbb{R}^{J_1 J_2 \times K_1 K_2}$, there exist two sets of matrices, $\{\mathbf{M}_1^{(r)}\}_{r=1}^R \subseteq \mathbb{R}^{J_1 \times K_1}$ and $\{\mathbf{M}_2^{(r)}\}_{r=1}^R \subseteq \mathbb{R}^{J_2 \times K_2}$, such that*

$$\mathbf{W} = \sum_{r=1}^R \mathbf{M}_1^{(r)} \otimes \mathbf{M}_2^{(r)}. \quad (3.1)$$

We note that Thm. 3.1 is a direct composition of the Kronecker-product SVD described in [45, Thm. 12.3.1].

According to Thm. 3.1, it is clear that the spatial degradation matrix \mathbf{D} can be decomposed into the sum of R Kronecker products. The validity of Asm. 2.1 then reduces as to whether R can equal 1. In other words, we need to determine the minimum value of R in the KD of \mathbf{D} . To this end, we define Kronecker rank:

Definition 3.1 (Kronecker Rank). *The Kronecker rank of matrix $\mathbf{W} \in \mathbb{R}^{J_1 J_2 \times K_1 K_2}$, denoted as $\text{kr}(J_1, K_1)_{\mathbf{W}}$, is defined as the minimal R such that R pairs of matrices generate the KD of \mathbf{W} as in (3.1).*

The issue then becomes how to determine $\text{kr}_{\mathbf{D}}^1$. In response, we recall that the spatial-degradation matrix \mathbf{D} models the process of blurring and downsampling; thus, the spatial degradation in (2.5) can be further elaborated as

$$\mathbf{X}_{[3]} = \mathbf{Z}_{[3]} \mathbf{D} = ((\mathcal{Z} * \Phi)_{\downarrow})_{[3]}, \quad (3.2)$$

where $\Phi \in \mathbb{R}^{\phi \times \phi}$ is the spatial-blurring kernel, $*$ denotes the periodic 2D convolution, and the subscript \downarrow is uniform

1. For a better presentation, we shorten the notation for the Kronecker rank of $\mathbf{D} \in \mathbb{R}^{M_1 M_2 \times m_1 m_2}$. In the sequel, $\text{kr}_{\mathbf{D}} \triangleq \text{kr}(M_1, m_1)_{\mathbf{D}}$.

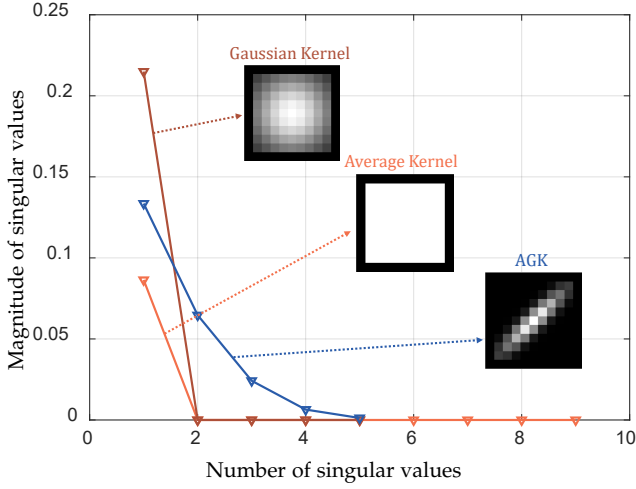


Fig. 1: The distribution singular values for some representative 9×9 blurring kernels.

downsampling. As such, the degradation matrix \mathbf{D} is endowed with significant structure and satisfies a wealth of properties. Accordingly, we have the following proposition.

Proposition 3.1. ² For the spatial-degradation matrix \mathbf{D} in (2.5), since it is physically modeled as (3.2), we have

$$\text{kr}_D = \text{rank} \{ \Phi \}. \quad (3.3)$$

The proof of Prop. 3.1 can be found in the supplemental material. We conclude from Prop. 3.1 that Asm. 2.1 holds true if and only if $\text{rank} \{ \Phi \} = 1$, i.e., the feasibility of TF-HSR rests solely on the rank of the blurring kernel.

To gauge the likelihood of having unity rank $\{ \Phi \}$, we consider Fig. 1 which visualizes the distribution of the singular values of different blurring kernels. We note that the second singular values for the isotropic-Gaussian and average kernels drop sharply to zero, meaning these kernels are rank-1, thereby supporting the use of TF-HSR with them. However, for the more complicated AGK, the curve descends much more slowly, thus $\text{rank} \{ \Phi \} > 1$, and it is no longer reasonable to apply TF-HSR when such anisotropic kernels are in effect. Indeed, Sec. 5 shows empirically that the fusion performance of current TF-HSR-based approaches deteriorates significantly under AGK blurring. Thus, in the next section, we reformulate TF-HSR to accommodate more general blurring processes.

3.2 The Proposed GTF-HSR Framework

Thm. 3.1 and Proposition 3.1 have proved that the \mathbf{P}_1 and \mathbf{P}_2 in Asm. 2.1 do not necessarily exist. What exists instead is the KD of spatial-degradation matrix $\mathbf{D} \in \mathbb{R}^{M_1 M_2 \times m_1 m_2}$,

² We present its proof assuming the convolution operator in (3.2) is periodic. However, one can verify the same conclusion holds subject to aperiodic convolutions such as that with zero-padding strategy.

which means that there exist collections $\{ \mathbf{P}_1^{(r)} \}_{r=1}^{\text{kr}_D} \subseteq \mathbb{R}^{m_1 \times M_1}$ and $\{ \mathbf{P}_2^{(r)} \}_{r=1}^{\text{kr}_D} \subseteq \mathbb{R}^{m_2 \times M_2}$ such that

$$\mathbf{D} = \sum_{r=1}^{\text{kr}_D} (\mathbf{P}_2^{(r)} \otimes \mathbf{P}_1^{(r)})^T. \quad (3.4)$$

Incorporating this expansion into (2.5), we have

$$\begin{aligned} \mathbf{X}_{[3]} &= \mathbf{Z}_{[3]} \mathbf{D} \\ &= \mathbf{Z}_{[3]} \sum_{r=1}^{\text{kr}_D} (\mathbf{P}_2^{(r)} \otimes \mathbf{P}_1^{(r)})^T \\ &= \sum_{r=1}^{\text{kr}_D} \mathbf{Z}_{[3]} (\mathbf{P}_2^{(r)} \otimes \mathbf{P}_1^{(r)})^T \\ &= \sum_{r=1}^{\text{kr}_D} \left(\mathcal{Z} \times_1 \mathbf{P}_1^{(r)} \times_2 \mathbf{P}_2^{(r)} \right)_{[3]}. \end{aligned} \quad (3.5)$$

Thus, we formulate a generalized version of TF-HSR, which we call GTF-HSR:

Definition 3.2 (GTF-HSR). Given HSI $\mathcal{X} \in \mathbb{R}^{m_1 \times m_2 \times S}$, MSI $\mathcal{Y} \in \mathbb{R}^{M_1 \times M_2 \times s}$, spectral-degradation matrix $\mathbf{R} \in \mathbb{R}^{s \times S}$, and spatial-degradation matrices $\{ \mathbf{P}_1^{(r)} \}_{r=1}^{\text{kr}_D} \subseteq \mathbb{R}^{m_1 \times M_1}$ and $\{ \mathbf{P}_2^{(r)} \}_{r=1}^{\text{kr}_D} \subseteq \mathbb{R}^{m_2 \times M_2}$ with $m_1 < M_1$, $m_2 < M_2$, and $s < S$, the GTF-HSR problem seeks the most appropriate SRI $\mathcal{Z} \in \mathbb{R}^{M_1 \times M_2 \times S}$ such that

$$\begin{aligned} \mathcal{X} &= \sum_{r=1}^{\text{kr}_D} \mathcal{Z} \times_1 \mathbf{P}_1^{(r)} \times_2 \mathbf{P}_2^{(r)}, \\ \mathcal{Y} &= \mathcal{Z} \times_3 \mathbf{R} \end{aligned} \quad (3.6)$$

The proposed GTF-HSR differs from the existing TF-HSR approaches in that it extends the modeling of spatial degradation from SRI to HSI into a summation form. Sec. 3.1 guarantees that such extension enables the GTF-HSR to accurately capture the real spatial-degradation process. Strictly speaking, GTF-HSR is equivalent to MF-HSR in the sense that any degradation process modeled by (2.5) can also be modeled by (3.6), and vice versa. However, such equivalence is not guaranteed between the TF-HSR and MF-HSR due to the failure of Asm. 2.1 to hold for general spatial-blurring of rank greater than unity.

3.3 Recoverability in GTF-HSR

Because of the ill-posedness of HSR, a solution satisfying (2.5), (2.6), or the proposed (3.6) does not necessarily recover the desired original SRI \mathcal{Z} . Thus, recoverability—i.e., the conditions for the solution to MF-HSR, TF-HSR, or GTF-HSR to surely obtain the ground-truth SRI \mathcal{Z} —plays a pivotal role in HSR. Consequently, although MF-HSR has been quite successful from an algorithmic perspective, one of the key motivations for proposing GTF-HSR is that the algebraic properties of tensors facilitate the establishing of recoverability conditions. That said, previous analyses (e.g., [28], [30], [31]) establishing recoverability of TF-HSR no longer apply due to the generalization of (2.1) as (3.4). Thus, we present a new recoverability analysis tailored to the

proposed GTF-HSR based on the block-term decomposition outlined in [43]:

Theorem 3.2. *Suppose the SRI $\mathcal{Z} \in \mathbb{R}^{M_1 \times M_2 \times S}$, HSI $\mathcal{X} \in \mathbb{R}^{m_1 \times m_2 \times S}$, and MSI $\mathcal{Y} \in \mathbb{R}^{M_1 \times M_2 \times s}$ satisfy relationship (2.5). Suppose further that the Tucker decomposition of \mathcal{Z} and the KD of spatial-degradation matrix $\mathbf{D} \in \mathbb{R}^{M_1 M_2 \times m_1 m_2}$ are*

$$\mathcal{Z} = \mathcal{G} \times_1 \mathbf{U}_1 \times_2 \mathbf{U}_2 \times_3 \mathbf{U}_3, \quad (3.7)$$

$$\mathbf{D} = \sum_{r=1}^{\text{kr}_{\mathbf{D}}} (\mathbf{P}_2^{(r)} \otimes \mathbf{P}_1^{(r)})^T, \quad (3.8)$$

where $\mathcal{G} \in \mathbb{R}^{L_1 \times L_2 \times C}$ is drawn from an absolutely continuous distribution; and \mathbf{U}_1 , \mathbf{U}_2 , and \mathbf{U}_3 have full column rank. Then, if it is true that

$$\begin{aligned} L_1 &\leq L_2 C, \quad L_2 \leq L_1 C, \quad S \geq 3 \\ \text{rank} \left\{ \left[\mathbf{P}_1^{(1)} \mathbf{U}_1, \dots, \mathbf{P}_1^{(\text{kr}_{\mathbf{D}})} \mathbf{U}_1 \right] \right\} &= L_1 \text{kr}_{\mathbf{D}}, \\ \text{rank} \left\{ \left[\mathbf{P}_2^{(1)} \mathbf{U}_2, \dots, \mathbf{P}_2^{(\text{kr}_{\mathbf{D}})} \mathbf{U}_2 \right] \right\} &= L_2 \text{kr}_{\mathbf{D}}, \quad (3.9) \\ \text{rank} \left\{ \mathbf{Y}_{[1]} \right\} &= L_1, \\ \text{rank} \left\{ \mathbf{Y}_{[2]} \right\} &= L_2, \end{aligned}$$

any solution of Tucker-rank at most (L_1, L_2, S) to GTF-HSR recovers SRI \mathcal{Z} with probability 1.

A proof of Thm. 3.2 built primarily on the properties of the block-term decomposition described in [43] can be found in the supplemental material. We note that, when $\text{kr}_{\mathbf{D}} = 1$, this theorem addresses the special case of the recoverability of TF-HSR. The main suppositions in this case include the rank constraints on the spatial dimensions of both the SRI and HSI images, as well as the genericity of the Tucker factors, which are common conditions that have been considered before [28], [30], [31]. Thus, from this perspective, Thm. 3.2 does not rely on unrealistic assumptions. More importantly, however, when $\text{kr}_{\mathbf{D}} > 1$, Thm. 3.2 addresses the recoverability of GTF-HSR, which is unprecedented in the literature.

While Thm. 3.2 guarantees that the proposed GTF-HSR can exactly recover SRI \mathcal{Z} , it can be shown that TF-HSR cannot recover \mathcal{Z} under the same conditions. That is, although Sec. 3.1 has already established that, when $\text{kr}_{\mathbf{D}} > 1$, it is impossible for Asm. 2.1 to hold, since HSR is a severely ill-posed problem, one might think that, as long as

$$\text{col} \left\{ \mathbf{D} - (\mathbf{P}_2 \otimes \mathbf{P}_1)^T \right\} \subseteq \text{null} \left\{ \mathbf{Z}_{[3]} \right\}, \quad (3.10)$$

there might still be hope of recovering \mathcal{Z} via TF-HSR. In other words, from the perspective of fusion performance, it might not be strictly necessary to precisely model the real spatial-degradation process. However, the following corollary, a simple consequence of Thm. 3.2, indicates that this is not the case.

Corollary 3.1. *Under the conditions of Thm. 3.2, if it is true that*

$$\begin{aligned} L_1 &\leq L_2 C, \quad L_2 \leq L_1 C, \quad S \geq 3 \\ \text{rank} \left\{ \left[\mathbf{P}_1^{(1)} \mathbf{U}_1, \dots, \mathbf{P}_1^{(\text{kr}_{\mathbf{D}})} \mathbf{U}_1 \right] \right\} &= L_1 \text{kr}_{\mathbf{D}}, \quad (3.11) \\ \text{rank} \left\{ \left[\mathbf{P}_2^{(1)} \mathbf{U}_2, \dots, \mathbf{P}_2^{(\text{kr}_{\mathbf{D}})} \mathbf{U}_2 \right] \right\} &= L_2 \text{kr}_{\mathbf{D}}, \end{aligned}$$

then any solution to TF-HSR recovers SRI \mathcal{Z} with probability 0 when $\text{kr}_{\mathbf{D}} > 1$.

A proof of Cor. 3.1 can be found in the supplemental material. We note that Cor. 3.1 indicates that, under a subset of the conditions of Thm. 3.2, TF-HSR will fail to recover \mathcal{Z} . Indeed, even in those cases wherein the conditions in Cor. 3.1 do not hold and applying TF-HSR is still theoretically possible, there exists no clear practical route to obtaining appropriate \mathbf{P}_1 or \mathbf{P}_2 that satisfy (3.10). Hence, the proposed GTF-HSR is at an advantage over TF-HSR, both in theory and in practice.

3.4 Blind HSR

An additional key advantage of the proposed GTF-HSR is its ability to facilitate blind HSR. As mentioned above, blind HSR, wherein the spatial-degradation matrix is unknown, is more realistic in certain settings but is an as-yet unresolved problem for TF-oriented methods, due to the lack of a process for acquiring a pair of appropriate \mathbf{P}_1 and \mathbf{P}_2 . Several strategies have been proposed in an attempt to circumvent this TF-HSR limitation—for example, [28], [30], [31], [32], [46] propose absorbing the spatial-degradation matrices into the factors to be estimated, inevitably resulting in suboptimal performance due to the resulting information loss. Alternatively, [32], [34], [47] conduct trial-and-error estimation. They directly utilize the rank-1 estimation of the blurring kernel to generate \mathbf{P}_1 and \mathbf{P}_2 to perform blind HSR. Yet, it is unclear if such scheme delivers the best estimation on the spatial degradation process. Moreover, there exists no means to determine if the spatial degradation process can be precisely modeled following TF-HSR.

In contrast, GTF-HSR confirms that precisely modeling the spatial degradation process following TF-HSR is impossible, and realizes this goal by invoking KD. That is, once we obtain an estimate of \mathbf{D} (using, e.g., appropriate methods developed for the MF-HSR problem), we can perform KD on \mathbf{D} to derive $\left\{ \mathbf{P}_1^{(r)} \right\}_{r=1}^{\text{kr}_{\mathbf{D}}} \subseteq \mathbb{R}^{m_1 \times M_1}$, and $\left\{ \mathbf{P}_2^{(r)} \right\}_{r=1}^{\text{kr}_{\mathbf{D}}} \subseteq \mathbb{R}^{m_2 \times M_2}$. Alternatively, we could develop methods to directly estimate the sets of these matrices since GTF-HSR is equivalent to MF-HSR in the sense of spatial-degradation modeling.

4 A GROUP-SPARSE SOLUTION FOR GTF-HSR

While Thm. 3.2 guarantees perfect SRI recovery is possible within the GTF-HSR framework, it does not actually indicate how one goes about effectuating the same. Consequently, we now proceed to develop an algorithmic procedure to solve GTF-HSR in the form of a factor-identification problem. While various tensor-decomposition frameworks could be used for this, we adopt the Tucker decomposition. That is, by applying the Tucker decomposition of (2.1) to (3.6), GTF-HSR becomes the problem of estimating the most appropriate $\mathcal{G} \in \mathbb{R}^{L_1 \times L_2 \times C}$, $\mathbf{U}_1 \in \mathbb{R}^{M_1 \times L_1}$, $\mathbf{U}_2 \in \mathbb{R}^{M_2 \times L_2}$, and $\mathbf{U}_3 \in \mathbb{R}^{S \times C}$ such that

$$\begin{aligned} \mathcal{X} &= \sum_{r=1}^{\text{kr}_{\mathbf{D}}} \mathcal{G} \times_1 \mathbf{P}_1^{(r)} \mathbf{U}_1 \times_2 \mathbf{P}_2^{(r)} \mathbf{U}_2 \times_3 \mathbf{U}_3, \quad (4.1) \\ \mathcal{Y} &= \mathcal{G} \times_1 \mathbf{U}_1 \times_2 \mathbf{U}_2 \times_3 \mathbf{R} \mathbf{U}_3, \end{aligned}$$

given HSI $\mathcal{X} \in \mathbb{R}^{m_1 \times m_2 \times S}$, MSI $\mathcal{Y} \in \mathbb{R}^{M_1 \times M_2 \times s}$, spatial degradations $\{\mathbf{P}_1^{(r)}\}_{r=1}^{\text{kr}_D} \subseteq \mathbb{R}^{m_1 \times M_1}$ and $\{\mathbf{P}_2^{(r)}\}_{r=1}^{\text{kr}_D} \subseteq \mathbb{R}^{m_2 \times M_2}$, and spectral degradation $\mathbf{R} \in \mathbb{R}^{s \times S}$.

4.1 Tensor Blockwise Group Sparsity

While the ill-posedness of HSR is the greatest obstacle to obtaining the ideal solution, under the Tucker decomposition, the SRI exhibits a wealth of properties that can be exploited to design regularizations that narrow down the solution set. Particularly, sparsity of the core tensor \mathcal{G} has been considered for HSR in the past (e.g., [26], [29], [46]). However, it has been observed (e.g., [48]) that real-world data often exhibits structured sparsity due to relationships contained within the data. Indeed, such structured sparsity can be seen prominently in the core tensor of a real HSI in Fig. 2(a). Consequently, we adopt blockwise group sparsity (BGS)—illustrated in Fig. 2(b)—as a prior for solving GTF-HSR rather than the simple sparsity used previously for HSR in [26], [29], [46]. Briefly, in BGS, the overall tensor is divided into smaller subblocks under the supposition that only a relative few of the subblocks contain nonzero samples; this is likely to be true if the subblocks are of sufficiently small size. We note that, while BGS has been used in the past [33], [49], [33] defines BGS for 4-order image cube cluster, which is difficult to be generalized towards an N -order tensor, including the 3-order tensor in our case. The semi-algebraic [49] is hard to deploy in our multi-sourced reconstruction problem. In response, we present a generalized BGS pattern for any N -order tensor achieved by an optimization-based algorithmic framework.

Our solution procedure effectively consists of imposing a BGS constraint onto the core tensor and casting the restoration task as a regularized optimization. To this end, we first propose an unfolding strategy appropriate for BGS which is defined below and also illustrated in Fig. 3.

Definition 4.1 (Blockwise Unfolding (B-Unfolding)). *For an N -order tensor $\mathcal{T} \in \mathbb{R}^{T_1 \times T_2 \times \dots \times T_N}$ with $T_n = t_n s_n$, $n = 1, 2, \dots, N$, its Blockwise unfolding, denoted by $\mathbf{T}_{[\mathbf{t}]}$, is defined as*

$$\mathbf{T}_{[\mathbf{t}]} = \text{reshape}\left(\text{permute}\left(\text{reshape}\left(\mathcal{T}, [t_1, s_1, \dots, t_N, s_N], [1, 3, \dots, 2N-1, 2, 4, \dots, 2N]\right)\right), \prod_{n=1}^N t_n, [\]\right) \quad (4.2)$$

where $\mathbf{t} \triangleq [t_1, t_2, \dots, t_N]$.

Effectively, the proposed B-unfolding reorganizes each subblock of size $t_1 \times t_2 \times \dots \times t_N$ into a single column of a matrix. B-unfolding thus allows the transformation a BGS constraint on a tensor into a column-wise sparsity constraint on its B-unfolding. We note that the latter has been well-studied extensively in prior literature and incorporated into optimizations in the form of the $\ell_{2,0}$ -norm, the number of nonzero columns in a matrix.

Thus, our proposed BGS-based approach yields the optimization

$$\begin{aligned} & \min_{\mathcal{G}, \mathbf{U}_1, \mathbf{U}_2, \mathbf{U}_3} \|\mathbf{G}_{[\mathbf{t}]}\|_{2,0} \\ \text{s.t. } & \mathcal{X} = \sum_{r=1}^{\text{kr}_D} \mathcal{G} \times_1 \mathbf{P}_1^{(r)} \mathbf{U}_1 \times_2 \mathbf{P}_2^{(r)} \mathbf{U}_2 \times_3 \mathbf{U}_3, \\ & \mathcal{Y} = \mathcal{G} \times_1 \mathbf{U}_1 \times_2 \mathbf{U}_2 \times_3 \mathbf{R} \mathbf{U}_3. \end{aligned} \quad (4.3)$$

One major benefit of using B-unfolding is that it enables the exploration of the multi-linear structure of higher-order data through a single compact norm. In spite of the consensus on the existence of multi-linearity in higher-order tensors, previous studies (e.g., [50], [51], [52]) have resorted to imposing constraints in the form of a summation or product of multiple norms, which inevitably increases model complexity and poses additional challenges for subsequent optimization procedures. In contrast, the proposed BGS constraint can easily balance the multi-linear structure hidden in the data through manipulating the parameter \mathbf{t} while reducing optimization burden, since it can be achieved by a single matrix norm.

That said, since the $\ell_{2,0}$ -norm is discontinuous and non-convex, the optimization in (4.3) is NP-hard [48]. While a straightforward solution would be to adopt a convex relaxation via the $\ell_{2,1}$ -norm, this would be intrinsically suboptimal since the $\ell_{2,1}$ -norm is the convex envelope of the $\ell_{2,0}$ -norm. Rather, we propose to use a nonconvex surrogate if the form of the Laplace function [48]; i.e.,

$$\|\mathbf{G}_{[\mathbf{t}]}\|_{2,0} \approx \|\mathbf{G}_{[\mathbf{t}]}\|_{2,\gamma} \triangleq \sum_i \left[1 - \exp\left(-\|\mathbf{g}_{[\mathbf{t}]}^{(i)}\|_2 / \gamma\right)\right], \quad (4.4)$$

where $\gamma > 0$ is a parameter to adjust the position of this surrogate function, $\mathbf{g}_{[\mathbf{t}]}^{(i)}$ is column i of matrix $\mathbf{G}_{[\mathbf{t}]}$, and we note that $\lim_{\gamma \rightarrow 0^+} \|\mathbf{G}_{[\mathbf{t}]}\|_{2,\gamma} = \|\mathbf{G}_{[\mathbf{t}]}\|_{2,0}$. Despite the fact that nonconvex regularized tensor approaches for data restoration have been, to some extent, studied before (e.g., [52], [53], [54], [55]), these past efforts have largely aimed at single-source restoration such as tensor completion, deconvolution, and denoising. In the multi-source case considered in this work, the optimization problem must be conducted at a much larger scale due to the increased amount of data. Such large-scale optimization is ill-handled by existing non-convex schemes, and, consequently, nonconvex surrogates have not been used for tensor-based HSR before now, to the best of our knowledge.

4.2 The Proposed BGS-GTF-HSR Algorithm

Using the Laplace surrogate, the HSR problem of (4.3) is relaxed into

$$\begin{aligned} & \min_{\mathcal{G}, \mathbf{U}_1, \mathbf{U}_2, \mathbf{U}_3} \|\mathbf{G}_{[\mathbf{t}]}\|_{2,\gamma} \\ \text{s.t. } & \mathcal{X} = \sum_{r=1}^{\text{kr}_D} \mathcal{G} \times_1 \mathbf{P}_1^{(r)} \mathbf{U}_1 \times_2 \mathbf{P}_2^{(r)} \mathbf{U}_2 \times_3 \mathbf{U}_3, \\ & \mathcal{Y} = \mathcal{G} \times_1 \mathbf{U}_1 \times_2 \mathbf{U}_2 \times_3 \mathbf{R} \mathbf{U}_3. \end{aligned} \quad (4.5)$$

This is a problem of a nonconvex objective function with multi-variable nonconvex constraints. Though alternating direction method of multipliers (ADMM) has seen success [53] in dealing with such problems, due to a larger scale

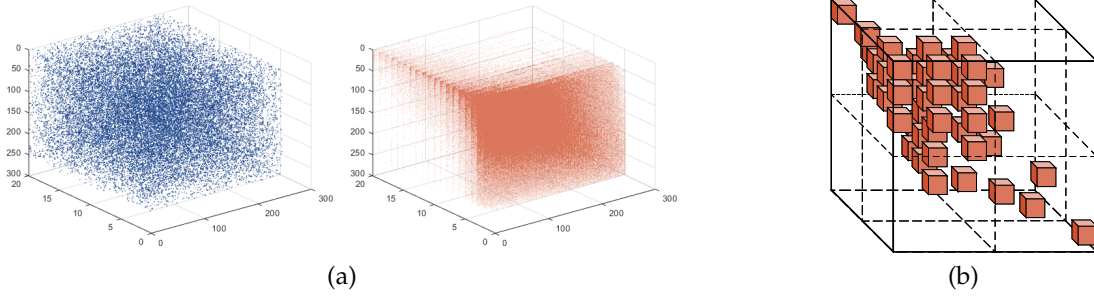


Fig. 2: (a) A sparse random tensor (left) vs. the core tensor from the Tucker decomposition of a real HSI (right); the core tensor (right) exhibits a prominent structured-sparsity characteristic. (b) A BGS tensor wherein sparsity takes on a blockwise structure.

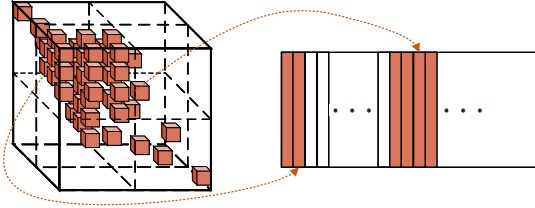


Fig. 3: B-unfolding, reorganizing each tensor block into a single column of a matrix.

here, some of our initial trials have indicated that directly applying ADMM to (4.5) may lead to a suboptimal solution and weak convergence. As an alternative, we devise a two-stage framework, which we refer to as BGS-GTF-HSR, to solve (4.5) in a divide-and-conquer manner: first, a subspace-identification problem which identifies \mathbf{U}_1 , \mathbf{U}_2 , and \mathbf{U}_3 , followed by a coding problem to identify \mathcal{G} . We develop BGS-GTF-HSR throughout the rest of this section.

4.2.1 Subspace Identification

We first seek a practical technique to identify \mathbf{U}_1 , \mathbf{U}_2 , and \mathbf{U}_3 , the subspace factors. Since the observed MSI \mathcal{Y} is degraded only spectrally, we derive \mathbf{U}_1 and \mathbf{U}_2 primarily from \mathcal{Y} while including a few supplementary basis vectors from HSI \mathcal{X} . That is, the spatial factors $\mathbf{U}_i \in \mathbb{R}^{M_i \times L_i}$, $i = 1, 2$ are partitioned into $\mathbf{U}_i = [\mathbf{U}_i^{\mathcal{Y}} \quad \mathbf{U}_i^{\mathcal{X}}]$ where $\mathbf{U}_i^{\mathcal{Y}} \in \mathbb{R}^{M_i \times K_i}$ with $K_i \gg L_i - K_i$. Through mode- i unfolding, we have

$$\mathbf{Y}_{[i]} = [\mathbf{U}_i^{\mathcal{Y}} \quad \mathbf{U}_i^{\mathcal{X}}] \mathbf{G}_{[i]} (\mathbf{R}\mathbf{U}_3 \otimes \mathbf{U}_{[3-i]})^T. \quad (4.6)$$

Now, suppose the columns of $\mathbf{U}_i^{\mathcal{Y}}$ span $\text{col}\{\mathbf{Y}_{[i]}\}$. We can then estimate $\mathbf{U}_i^{\mathcal{Y}}$ via

$$[\mathbf{U}_i^{\mathcal{Y}}, \sim, \sim] = \text{svd}(\mathbf{Y}_{[i]}, K_i). \quad (4.7)$$

We extract $\mathbf{U}_i^{\mathcal{X}}$ from HSI \mathcal{X} . Again by mode- i unfolding, we have

$$\mathbf{X}_{[i]} = [\mathbf{P}_i^{(1)} \quad \dots \quad \mathbf{P}_i^{(\text{krD})}] (\mathbf{I}_{\text{krD}} \otimes [\mathbf{U}_i^{\mathcal{Y}} \quad \mathbf{U}_i^{\mathcal{X}}]) \mathbf{A}_i \quad (4.8)$$

where

$$\mathbf{A}_i = \begin{bmatrix} \mathbf{G}_{[i]} \left(\mathbf{U}_3 \otimes \mathbf{P}_{3-i}^{(1)} \mathbf{U}_{3-i} \right) \\ \mathbf{G}_{[i]} \left(\mathbf{U}_3 \otimes \mathbf{P}_{3-i}^{(2)} \mathbf{U}_{3-i} \right) \\ \vdots \\ \mathbf{G}_{[i]} \left(\mathbf{U}_3 \otimes \mathbf{P}_{3-i}^{(\text{krD})} \mathbf{U}_{3-i} \right) \end{bmatrix}. \quad (4.9)$$

Algorithm 1 BGS-GTF-HSR: Subspace Identification

Input: The observed HSI $\mathcal{X} \in \mathbb{R}^{m_1 \times m_2 \times S}$, MSI $\mathcal{Y} \in \mathbb{R}^{M_1 \times M_2 \times s}$, spatial-degradation matrices $\{\mathbf{P}_1^{(r)}\}_{r=1}^{\text{krD}} \subseteq \mathbb{R}^{M_1 \times M_1}$ and $\{\mathbf{P}_2^{(r)}\}_{r=1}^{\text{krD}} \subseteq \mathbb{R}^{M_2 \times M_2}$, spectral-degradation matrix $\mathbf{R} \in \mathbb{R}^{s \times S}$, μ, ϵ, K_1, K_2
Output: Subspace factors $\mathbf{U}_1 \in \mathbb{R}^{M_1 \times L_1}$, $\mathbf{U}_2 \in \mathbb{R}^{M_2 \times L_2}$, $\mathbf{U}_3 \in \mathbb{R}^{S \times C}$

- 1: **for** $i = 1 : 2$ **do**
- 2: $[\mathbf{U}_i^{\mathcal{Y}}, \sim, \sim] = \text{svd}(\mathbf{Y}_{[i]}, K_i)$
- 3: initialize $\rho, \rho_{\max}, \nu > 1$, choose random \mathbf{A}_i
- 4: set $\mathbf{B}_i = \mathbf{A}_i$, $\mathbf{U}_i^{\mathcal{X}} = \mathbf{0}$, $\mathbf{M}_i = \mathbf{0}$
- 5: **while** $\frac{\|\mathbf{U}_i^{\mathcal{X}} - \mathbf{U}_i^{\mathcal{X}(\text{previous})}\|_F}{\|\mathbf{U}_i^{\mathcal{X}(\text{previous})}\|_F} \geq \epsilon$ **do**
- 6: $\tilde{\mathbf{X}}_{[i]} \leftarrow \mathbf{X}_{[i]} - \sum_{r=1}^{\text{krD}} \mathbf{P}_i^{(r)} \mathbf{U}_i^{\mathcal{Y}} \mathbf{B}_i^{(r)\mathcal{Y}}$
- 7: Update $\mathbf{U}_i^{\mathcal{X}}$ by solving $\nabla \mathcal{L}_{\mathbf{U}_i^{\mathcal{X}}} = 0$ via conjugate gradient (CG) [45]
- 8: $\mathbf{D}_i \leftarrow [\mathbf{P}_i^{(1)} \quad \dots \quad \mathbf{P}_i^{(\text{krD})}] (\mathbf{I}_{\text{krD}} \otimes [\mathbf{U}_i^{\mathcal{Y}} \quad \mathbf{U}_i^{\mathcal{X}}])$
- 9: $\mathbf{B}_i \leftarrow (\mathbf{D}_i^T \mathbf{D}_i + \frac{\rho}{2} \mathbf{I}_{L_i \text{krD}})^{-1} \left(\mathbf{D}_i^T \mathbf{X}_{[i]} + \frac{\rho}{2} \left(\mathbf{A}_i + \frac{\mathbf{M}_i}{\rho} \right) \right)$
- 10: $\mathbf{A}_i \leftarrow \text{soft} \left(\mathbf{B}_i - \frac{\mathbf{M}_i}{\rho}, \frac{\mu}{\rho} \right)$
- 11: $\mathbf{M}_i \leftarrow \mathbf{M}_i + \rho(\mathbf{A}_i - \mathbf{B}_i)$
- 12: $\rho \leftarrow \min\{\nu\rho, \rho_{\max}\}$
- 13: **end while**
- 14: $[\mathbf{U}_3, \sim, \sim] = \text{svd}(\mathbf{X}_{[3]}, C)$
- 15: **end for**

The degradation matrices $\{\mathbf{P}_i^{(r)}\}_{r=1}^{\text{krD}}$ hinder direct extraction of $\mathbf{U}_i^{\mathcal{X}}$ from $\text{col}\{\mathbf{X}_{[i]}\}$; therefore, we propose to impose a sparse constraint on \mathbf{A} to estimate $\mathbf{U}_i^{\mathcal{X}}$ via sparse dictionary learning,

$$\begin{aligned} \min_{\mathbf{U}_i^{\mathcal{X}}, \mathbf{A}_i} & \|\mathbf{X}_{[i]} - \\ & [\mathbf{P}_i^{(1)} \quad \dots \quad \mathbf{P}_i^{(\text{krD})}] (\mathbf{I}_{\text{krD}} \otimes [\mathbf{U}_i^{\mathcal{Y}} \quad \mathbf{U}_i^{\mathcal{X}}]) \mathbf{B}_i\|_F^2 + \mu \|\mathbf{A}_i\|_1 \\ \text{s.t. } & \mathbf{A}_i = \mathbf{B}_i, \end{aligned} \quad (4.10)$$

where we have introduced auxiliary variables \mathbf{B}_i . The optimization (4.10) is solved via ADMM; this is described in detail in the supplemental material.

While we could estimate spectral subspace factor \mathbf{U}_3 in a similar fashion as is done above for the spatial factors, we instead adopt the simpler approach of extracting \mathbf{U}_3 directly from the HSI \mathcal{X} as it is subject to only spatial degradation:

$$[\mathbf{U}_3, \sim, \sim] = \text{svd}(\mathbf{X}_{[3]}, C). \quad (4.11)$$

The subspace-identification procedure is presented as Alg. 1 wherein $\mathbf{B}_i^{(r)\mathcal{Y}} \in \mathbb{R}^{K_i \times m_{3-i}S}$ and $\mathbf{B}_i^{(r)\mathcal{X}} \in \mathbb{R}^{(L_i - K_i) \times m_{3-i}S}$ are submatrices partitioned from \mathbf{B}_i as $\mathbf{B}_i = [(\mathbf{B}_i^{(1)\mathcal{Y}})^T \ (\mathbf{B}_i^{(1)\mathcal{X}})^T \ \dots \ (\mathbf{B}_i^{(\text{kr}_D)\mathcal{Y}})^T \ (\mathbf{B}_i^{(\text{kr}_D)\mathcal{X}})^T]^T$; and, in step 7,

$$\nabla \mathcal{L}_{\mathbf{U}_i^{\mathcal{X}}} \triangleq \sum_{r_1=1}^{\text{kr}_D} \sum_{r_2=1}^{\text{kr}_D} \left(\mathbf{P}_i^{(r_1)} \right)^T \mathbf{P}_i^{(r_2)} \mathbf{U}_i^{\mathcal{X}} \mathbf{B}_i^{(r_2)\mathcal{X}} \left(\mathbf{B}_i^{(r_1)\mathcal{X}} \right)^T - \sum_{r=1}^{\text{kr}_D} \left(\mathbf{P}_i^{(r)} \right)^T \tilde{\mathbf{X}}_{[i]} \left(\mathbf{B}_i^{(r)\mathcal{X}} \right)^T. \quad (4.12)$$

4.2.2 BGS Coding

With the factor matrices \mathbf{U}_1 , \mathbf{U}_2 , and \mathbf{U}_3 being determined by Alg. 1, the sole remaining task in problem (4.5) is to determine \mathcal{G} . In doing so, we introduce auxiliary variables \mathcal{G}_r such that (4.5) becomes

$$\begin{aligned} & \min_{\{\mathcal{G}_r\}_{r=1}^{\text{kr}_D}, \mathcal{G}, \hat{\mathbf{G}}} \left\| \hat{\mathbf{G}} \right\|_{2,\gamma} \\ \text{s.t. } & \mathcal{X} = \sum_{r=1}^{\text{kr}_D} \mathcal{G}_r \times_1 \mathbf{P}_1^{(r)} \mathbf{U}_1 \times_2 \mathbf{P}_2^{(r)} \mathbf{U}_2 \times_3 \mathbf{U}_3, \\ & \mathcal{Y} = \mathcal{G} \times_1 \mathbf{U}_1 \times_2 \mathbf{U}_2 \times_3 \mathbf{R} \mathbf{U}_3, \\ & \hat{\mathbf{G}} = \mathbf{G}_{[t]}, \\ & \mathcal{G} = \mathcal{G}_r, \quad r = 1, 2, \dots, \text{kr}_D. \end{aligned} \quad (4.13)$$

The optimization is carried out via ADMM; thus, for brevity, we present only the resulting algorithm here as Alg. 2, relegating the complete details to the supplemental material. We do note, however, that, we solve the subproblem in step 16, which is critical to achieving the desired BGS pattern, via the recently developed generalized accelerating iterative (GAI) [48].

4.2.3 Complexity and Convergence

In Alg. 1, the main complexity lies in the CG iterations in step 7 and the matrix inversion in step 9. In the CG iterations, the primary computational burden is the multiplication of the system matrices with factor matrix, whose complexity is $\mathcal{O}(M_i(L_i - K_i) + M_i(L_i - K_i)^2)$, $i = 1, 2$. In step 9, the matrix inversion has complexity $\mathcal{O}(\text{kr}_D^3 L_i^3)$. Thus the total complexity of Alg. 1 is $\sum_{i=1}^2 [\mathcal{O}(N_{\text{CG}}(M_i(L_i - K_i) + M_i(L_i - K_i)^2)) + \mathcal{O}(\text{kr}_D^3 L_i^3)]$, where N_{CG} denotes the number of CG iterations.

In Alg. 2, the complexity centers mostly on the updating of \mathcal{G} , $\{\mathcal{G}_r\}_{r=1}^{\text{kr}_D}$, and $\hat{\mathbf{G}}$. Both the updating of \mathcal{G} and $\{\mathcal{G}_r\}_{r=1}^{\text{kr}_D}$ costs the same complexity, $\mathcal{O}(L_1^2 L_2 C + L_1 L_2^2 C + L_1 L_2 C^2)$, while the complexity of performing step 16 via GAI is $\mathcal{O}(\prod_{n=1}^3 s_n)$ where $\mathbf{s} = [s_1 \ s_2 \ s_3]$ is defined in Def. 4.1. As such, the whole complexity of Alg. 2 is $\mathcal{O}(\text{kr}_D(L_1^2 L_2 C + L_1 L_2^2 C + L_1 L_2 C^2)) + \mathcal{O}(N_{\text{GAI}} \prod_{n=1}^3 s_n)$, where N_{GAI} is the number of GAI iterations. Besides, we'd like to note that the

Algorithm 2 BGS-GTF-HSR: BGS Coding

Input: The observed HSI $\mathcal{X} \in \mathbb{R}^{m_1 \times m_2 \times S}$, MSI $\mathcal{Y} \in \mathbb{R}^{M_1 \times M_2 \times s}$, spatial-degradation matrices $\{\mathbf{P}_1^{(r)}\}_{r=1}^{\text{kr}_D} \subseteq \mathbb{R}^{m_1 \times M_1}$ and $\{\mathbf{P}_2^{(r)}\}_{r=1}^{\text{kr}_D} \subseteq \mathbb{R}^{m_2 \times M_2}$, spectral-degradation matrix $\mathbf{R} \in \mathbb{R}^{s \times S}$, subspace factors $\mathbf{U}_1 \in \mathbb{R}^{M_1 \times L_1}$, $\mathbf{U}_2 \in \mathbb{R}^{M_2 \times L_2}$, $\mathbf{U}_3 \in \mathbb{R}^{S \times C}$, λ, ϵ

Output: Core tensor $\mathcal{G} \in \mathbb{R}^{L_1 \times L_2 \times C}$

- 1: initialize $\rho, \rho_{\max}, \nu > 1$, choose random \mathbf{A}_i
- 2: set \mathcal{G} , $\{\mathcal{G}_r\}_{r=1}^{\text{kr}_D}$, $\mathcal{P}^{\mathcal{X}}$, $\mathcal{P}^{\mathcal{Y}}$, \mathbf{W} , $\{\mathcal{P}_r\}_{r=1}^{\text{kr}_D}$ to 0
- 3: **while** $\frac{\|\mathcal{G} - \mathcal{G}^{(\text{previous})}\|_F}{\|\mathcal{G}^{(\text{previous})}\|_F} \geq \epsilon$ **do**
- 4: **for** $r = 1 : \text{kr}_D$ **do**
- 5: $\mathcal{H} \leftarrow \mathcal{X} + \frac{\mathcal{P}^{\mathcal{X}}}{\rho} - \sum_{r^* \neq r} \mathcal{G}_{r^*} \times_1 \mathbf{P}_1^{(r^*)} \mathbf{U}_1 \times_2 \mathbf{P}_2^{(r^*)} \mathbf{U}_2 \times_3 \mathbf{U}_3$
- 6: $\mathbf{Q}_1 \leftarrow \mathbf{P}_1^{(r)} \mathbf{U}_1$, $\mathbf{Q}_2 \leftarrow \mathbf{P}_2^{(r)} \mathbf{U}_2$, $\mathbf{Q}_3 \leftarrow \mathbf{U}_3$
- 7: $\mathcal{K} \leftarrow \mathcal{H} + \frac{\mathcal{P}_r}{\rho}$
- 8: **for** $n = 1 : 3$ **do**
- 9: $[\mathbf{V}_n, \sqrt{\Sigma_n}, \sim] = \text{svd}(\mathbf{Q}_n^T)$
- 10: **end for**
- 11: $\mathcal{T} \leftarrow \mathcal{H} \times_1 \mathbf{Q}_1^T \times_2 \mathbf{Q}_2^T \times_3 \mathbf{Q}_3^T + \mathcal{K}$
- 12: $\mathcal{T}' \leftarrow \mathcal{T} \times_1 \mathbf{V}_1^T \times_2 \mathbf{V}_2^T \times_3 \mathbf{V}_3^T$
- 13: $\text{Vec}(\mathcal{T}'') \leftarrow (\Sigma_3 \otimes \Sigma_2 \otimes \Sigma_1 + \mathbf{I}_{L_1 L_2 C})^{-1} \text{Vec}(\mathcal{T}')$
- 14: $\mathcal{G}_r \leftarrow \mathcal{T}'' \times_1 \mathbf{V}_1 \times_2 \mathbf{V}_2 \times_3 \mathbf{V}_3$
- 15: **end for**
- 16: $\hat{\mathbf{G}} \leftarrow \arg \min_{\hat{\mathbf{G}}} \frac{\rho}{2} \left\| \hat{\mathbf{G}} - \mathbf{G}_{[t]} + \frac{\mathbf{W}}{\rho} \right\|_F^2 + \left\| \hat{\mathbf{G}} \right\|_{2,\gamma}$
- 17: $\mathcal{H} \leftarrow \mathcal{Y} + \frac{\mathcal{P}^{\mathcal{Y}}}{\rho}$, $\mathbf{Q}_1 \leftarrow \mathbf{U}_1$, $\mathbf{Q}_2 \leftarrow \mathbf{U}_2$, $\mathbf{Q}_3 \leftarrow \mathbf{R} \mathbf{U}_3$
- 18: $\mathcal{K} \leftarrow \frac{(\mathcal{G}^{\mathbf{W}} + \sum_{r=1}^{\text{kr}_D} \mathcal{G}_r - \frac{\mathcal{P}_r}{\rho})}{\text{kr}_D + 1}$, $\tau \leftarrow \text{kr}_D + 1$
- 19: **for** $n = 1 : 3$ **do**
- 20: $[\mathbf{V}_n, \sqrt{\Sigma_n}, \sim] = \text{svd}(\mathbf{Q}_n^T)$
- 21: **end for**
- 22: $\mathcal{T} \leftarrow \mathcal{H} \times_1 \mathbf{Q}_1^T \times_2 \mathbf{Q}_2^T \times_3 \mathbf{Q}_3^T + \tau \mathcal{K}$
- 23: $\mathcal{T}' \leftarrow \mathcal{T} \times_1 \mathbf{V}_1^T \times_2 \mathbf{V}_2^T \times_3 \mathbf{V}_3^T$
- 24: $\text{Vec}(\mathcal{T}'') \leftarrow (\Sigma_3 \otimes \Sigma_2 \otimes \Sigma_1 + \tau \mathbf{I}_{L_1 L_2 C})^{-1} \text{Vec}(\mathcal{T}')$
- 25: $\mathcal{G} \leftarrow \mathcal{T}'' \times_1 \mathbf{V}_1 \times_2 \mathbf{V}_2 \times_3 \mathbf{V}_3$
- 26: **end while**

matrices in step 13 and 24 requiring inversion are diagonal. Thus their inversion can be calculated by element-wise inversion on their diagonals. And the subsequent multiplication can also be done element-wisely. These two steps, though involving the inversion on large-scale matrices, do not add complexity to the overall algorithm.

Although ADMM has been widely deployed (e.g., [16], [29], [56]), its convergence has been confirmed for only 2-block convex problems [57]. Here, due to the larger scale of the problem, as well as the nonconvexity of both the constraint and objective function, convergence of the proposed BGS-GTF-HSR is not theoretically guaranteed. Nonetheless, we have not witnessed any convergence issues in our experimental evaluations.

5 EXPERIMENTAL STUDY

5.1 Experimental Setup

We now present a body of experimental results to evaluate the proposed BGS-GTF-HSR framework. Experiments using

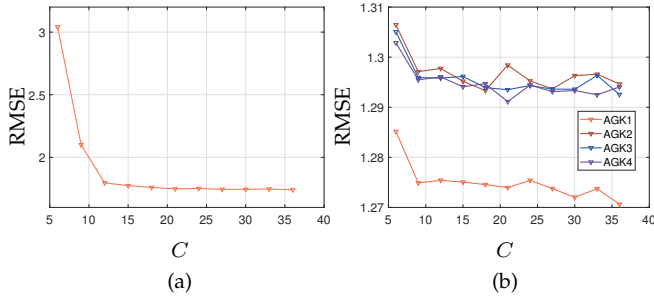


Fig. 4: Tuning process of spectral rank C in terms of RMSE. (a) URBAN dataset. (b) Houston2013 dataset.

both simulated and real datasets are conducted. In the simulated experiments, both degradation by the traditional IGK as well as the more realistic AGK are considered. Moreover, within the experiments for each kernel, both blind and non-blind HSR are employed to demonstrate the superiority of the proposed BGS-GTF-HSR. Since BGS-GTF-HSR is unsupervised, comparisons are made to only unsupervised techniques from prior literature; specifically, we compare to Hysure [13], SURE [23], LTMR [16], LRTA, [17], and ZSL [24] as MF-HSR methods³, and to STEREO [28], CSTF [29], and FSTRD [47] as TF-HSR methods. Note that, for STEREO, we use its blind version (B-STE) in the blind HSR experiments. For the remaining methods, the spatial-degradation matrices are estimated via the technique suggested in [13]. The proposed BGS-GTF-HSR is implemented in MATLAB R2021a on Intel[®] Core[™] i7-8700 CPU @ 3.20 GHz with 32-GB RAM. We measure performance in terms of peak signal-to-noise ratio (PSNR), root mean square error (RMSE), spectral angle mapper (SAM), and structural similarity metric (SSIM).

As for data, we employ the URBAN, Houston2013, and Houston2018 datasets. The URBAN dataset⁴ dataset is a 210-band HSI of 307×307 pixels at 2-m spatial resolution. The spectral coverage is 400–2,500 nm with a 10-nm sampling interval. Due to critical water vapor and atmospheric effects, bands 1–4, 76, 87, 101–111, 136–153, and 198–210 were discarded. The upper-left corner of the processed image was retained to obtain a $256 \times 256 \times 162$ SRI. The Houston2013 dataset⁵ is a hyperspectral image $349 \times 1905 \times 144$ spatial size at 2.5-m spatial resolution. The 144 spectral bands cover 380 nm to 1050 nm. With zero pixels being discarded, a $322 \times 1903 \times 144$ image cube forms the final ground truth; this is then partitioned into 20 overlapping $256 \times 256 \times 144$ subscenes as SRIs. Finally, the Houston2018 dataset⁶ consists of a real-world HSI-MSI pair. The HSI is of size $1,202 \times 4,172 \times 48$ and was acquired by an ITRES CASI 1500 sensor, covering wavelengths 380–1,050 nm at 1-m spatial resolution. The image is cropped to size $500 \times 500 \times 48$ for further processing. The $12,020 \times 11,920 \times 3$ MSI of

3. We note that, while LTMR and LRTA employ certain aspects of tensors—namely, tensor rank—their operation is more in line with the MF-HSR framework of (2.5) than the TF-HSR of (2.6); we thus treat them as MF-HSR techniques here.

4. <https://www.erd.c.usace.army.mil/Media/Fact-Sheets/Fact-Sheet-Article-View/Article/610433/hypercube/#>

5. https://hyperspectral.ee.uh.edu/?page_id=459

6. https://hyperspectral.ee.uh.edu/?page_id=1075

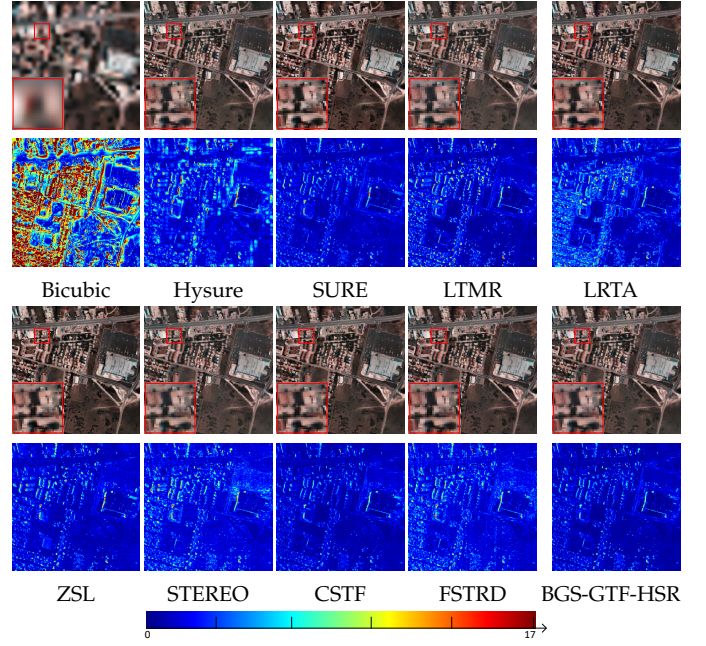


Fig. 5: Non-blind fusion results and error maps on the URBAN dataset with IGK. Pseudo-color is composed of bands 45, 20 and 10.

the pair was acquired by a DiMAC ULTRALIGHT+ at a very high spatial resolution of 5 cm. An area of the size $10,000 \times 10,000 \times 3$ that is registered with the HSI is then selected. Considering that the 20-times gap in the spatial resolution between the HSI and the MSI is too large for current fusion methods, and a size of $10,000 \times 10,000$ is also too large for the RAM of our machine, we perform five-times downsampling on the HSI and 25-times downsampling on the MSI to generate a data pair composed of a $100 \times 100 \times 48$ HSI at 5-m spatial resolution and a $400 \times 400 \times 3$ MSI at 1.25-m spatial resolution.

5.2 BGS-GTF-HSR Hyperparameters

The main hyperparameters concerning the proposed BGS-GTF-HSR include the latent Tucker-Rank (L_1, L_2, C) , the partition parameters K_1 and K_2 in Alg. 1, and the shape parameter $\mathbf{t} = [t_1, t_2, t_3]$ of the proposed B-unfolding deciding the specific BGS pattern of the core tensor. Since it is well-recognized that the HSI is not as low rank in the spatial domain as it is in the spectral domain, we set $L_1 = M_1$ and $L_2 = M_2$; that is, $L_1 = L_2 = 256$ for the simulated dataset, and $L_1 = L_2 = 400$ for the real Houston2018 HSI-MSI pair. Because the spatial information is largely preserved in the HSI, we set the ratio of K_i to $L_i - K_i$ to be 15 : 1 in order to have the atoms extracted from the MSI be dominant; that is, $K_1 = K_2 = 240$ for the simulated experiments, and $K_1 = K_2 = 375$ for the real experiments. As for the spectral rank C , we fine-tune it on both the URBAN and Houston2013 datasets as depicted in Fig. 4, setting $C = 12$ in consideration of both performance and computational efficiency. To determine the BGS shape parameter \mathbf{t} , we note that the size of the elementary block must be significantly smaller than the overall core tensor, and the spatial shape must be much larger than the spectral shape in accordance

TABLE 1: Performance on the URBAN dataset

Setup	Methods	Quality Indices			
		PSNR \uparrow	RMSE \downarrow	SAM \downarrow	SSIM \uparrow
Non-blind	Hysure	40.0915	3.3614	2.7795	0.9894
	SURE	42.4016	2.2118	1.8641	0.9911
	LTM	44.0306	2.3757	2.0022	0.9918
	LRTA	42.6566	3.2413	2.4486	0.9852
	ZSL	42.5588	2.3110	1.9789	0.9921
	STEREO	41.1537	2.7029	2.4912	0.9833
	CSTF	44.2222	1.8827	1.6649	0.9918
	FSTRD	41.7204	2.7526	2.4355	0.9848
	BGS-GTF-HSR	45.4533	1.7936	1.6218	0.9939
Blind	Hysure	40.1689	3.3059	2.7597	0.9895
	SURE	41.8384	2.3932	2.1031	0.9901
	LTM	43.9173	2.3898	2.0207	0.9917
	LRTA	42.5482	3.2605	2.4644	0.9850
	ZSL	42.7150	2.2951	1.9791	0.9923
	B-STE	39.7142	3.0233	2.7546	0.9800
	CSTF	43.6849	1.9766	1.8166	0.9909
	FSTRD	41.6403	2.7522	2.4419	0.9838
	BGS-GTF-HSR	44.6240	2.0684	1.7326	0.9926

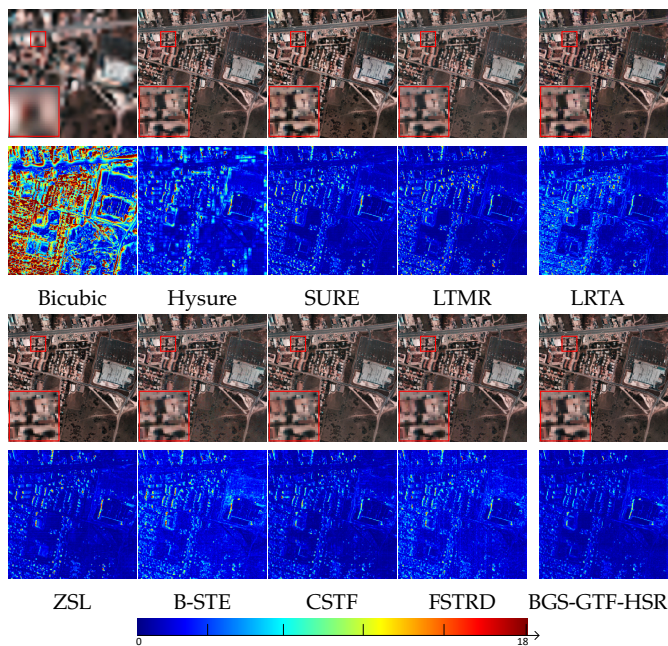


Fig. 6: Blind fusion results and error maps on URBAN dataset with IGK. Pseudo-color is composed of bands 45, 20 and 10.

with the lower rank in the spectral domain. These lead to the condition that $t_1 \ll L_1, t_2 \ll L_2$ and $t_1, t_2 \gg t_3$. Thus, we use $\mathbf{t} = [16, 16, 3]$ and $\mathbf{t} = [20, 20, 3]$ for the simulated and real experiments, respectively.

5.3 HSR with IGK

In the results presented in this section, we employ the URBAN dataset, using the SRI described in Sec. 5.1 as the ground truth and generating an HSI and MSI from in artificially. Specifically, we blurred the SRI with a 9×9 IGK

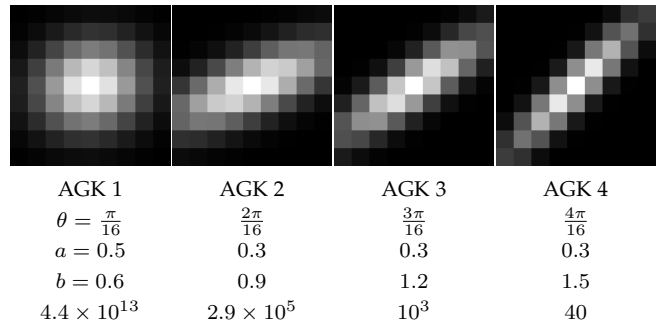


Fig. 7: The four AGK blurring kernels; the numbers in the last row are the condition number. θ, a, b are defined in Section 2.3.

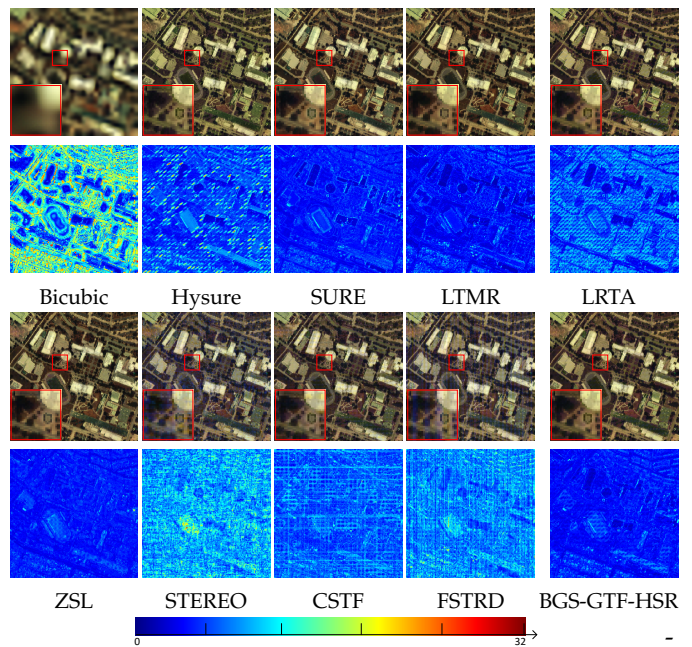


Fig. 8: Non-blind fusion results and error maps for the Houston2013 dataset with AGK 3 (Scene 2). Pseudo-color is composed of bands 30, 20 and 10.

with standard deviation 3.3973 and spatially downsampled it by a factor of 8 to simulate an HSI of size $32 \times 32 \times 162$. The $256 \times 256 \times 6$ MSI is generated by averaging the SRI bands falling into the wavelength between 450–520, 520–600, 630–690, 760–900, 1, 550–1750, and 2, 080–2, 350 nm to simulate the spectral coverage of the USGS/NASA Landsat7 satellite [29].

For non-blind performance, the degradation matrices are assumed to be known. Fig. 5 presents the fusion results for bands 30, 20, and 10 as pseudo-color images, along with corresponding error maps generated by pixel-wise SAM between the results and ground-truth SRI. Visually, the proposed BGS-GTF-HSR has the error map with the lowest brightness and least highlighted area, while SURE, ZSL, and CSTF yield competitive results. This conclusion is further confirmed by quantitative evaluation in Table 1—we note that the proposed BGS-GTF-HSR obtains the best values for all the metrics considered for non-blind performance.

Finally, we assess blind fusion performance, wherein

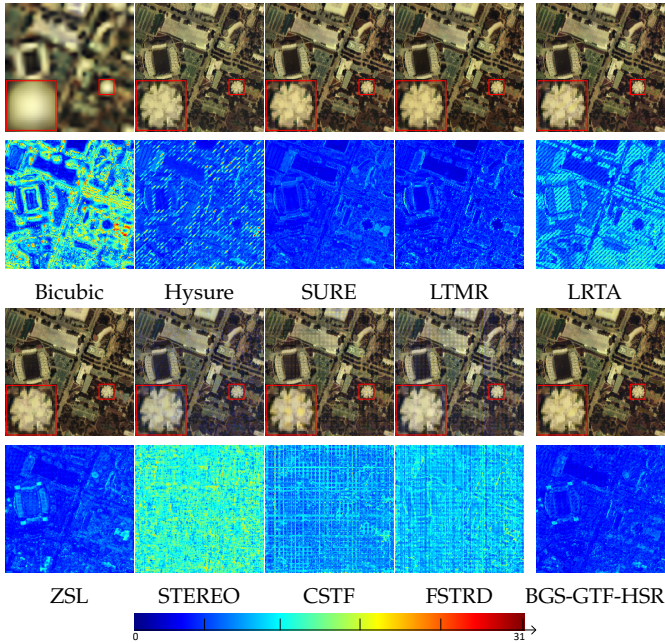


Fig. 9: Non-blind fusion results and error maps for the Houston2013 dataset with AGK 4 (Scene 5). Pseudo-color is composed of bands 30, 20 and 10.

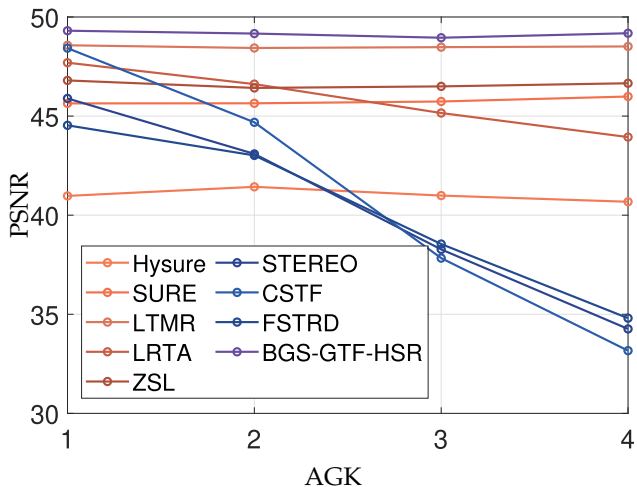


Fig. 10: PSNR performance for varying AGK (1 through 4) for the Houston2013 dataset, demonstrating how the methods respond to the increase in the rank of the blurring kernel.

the degradation matrices are unknown to the techniques. The corresponding visual results are given in Fig. 6 while quantitative performance is tabulated Table 1. We note that the fusion performance for all the techniques suffers under the blind scenario, as can be observed in both Table 1 and in the error maps of Fig. 6. However, the proposed BGS-GTF-HSR still outperforms other methods since it has the best values for most quantitative metrics, and its error map is darkest.

TABLE 2: Performance on the Houston2013 dataset with AGK 1 (averaged over 20 scenes)

Setup	Methods	Quality Indices			
		PSNR \uparrow	RMSE \downarrow	SAM \downarrow	SSIM \uparrow
Non-blind	Hysure	40.9721	2.6210	2.4319	0.9801
	SURE	45.6402	1.5051	1.4854	0.9877
	LTMR	48.5731	1.3353	1.3054	0.9903
	LRTA	47.6939	1.5624	1.6141	0.9876
	ZSL	46.7990	1.3749	1.3571	0.9920
	STEREO	45.8905	1.8110	1.9726	0.9786
	CSTF	48.4274	1.3367	1.4734	0.9893
	FSTRD	44.5336	2.3053	2.5005	0.9666
	BGS-GTF-HSR	49.3079	1.1857	1.2251	0.9919
Blind	Hysure	41.4202	2.5011	2.3992	0.9819
	SURE	45.3860	1.5556	1.5274	0.9871
	LTMR	48.2073	1.3768	1.3314	0.9901
	LRTA	48.3274	1.3811	1.4247	0.9898
	ZSL	45.4437	2.4206	2.3740	0.9616
	B-STE	44.4886	1.9713	2.1890	0.9770
	CSTF	46.8317	1.4326	1.4425	0.9899
	FSTRD	43.7708	2.4287	2.5701	0.9651
	BGS-GTF-HSR	49.2943	1.1832	1.2218	0.9918

TABLE 3: Performance on the Houston2013 dataset with AGK 2 (averaged over 20 scenes)

Setup	Methods	Quality Indices			
		PSNR \uparrow	RMSE \downarrow	SAM \downarrow	SSIM \uparrow
Non-blind	Hysure	41.4307	2.4503	2.3813	0.9805
	SURE	45.6455	1.4881	1.4758	0.9882
	LTMR	48.4367	1.3678	1.3320	0.9900
	LRTA	46.6136	1.8789	1.8861	0.9835
	ZSL	46.4207	1.4512	1.4595	0.9917
	STEREO	43.0912	2.4394	2.5337	0.9682
	CSTF	44.6860	1.8134	1.7637	0.9862
	FSTRD	43.0151	2.5345	2.6199	0.9624
	BGS-GTF-HSR	49.1637	1.2157	1.2544	0.9918
Blind	Hysure	41.2449	2.5472	2.4611	0.9806
	SURE	44.9667	1.7049	1.5805	0.9868
	LTMR	47.6852	1.5452	1.4171	0.9890
	LRTA	47.6156	1.6105	1.5690	0.9882
	ZSL	46.6373	1.4030	1.3796	0.9908
	B-STE	44.3812	1.9979	2.2201	0.9764
	CSTF	46.1899	1.6083	1.5634	0.9881
	FSTRD	43.2479	2.5325	2.6075	0.9637
	BGS-GTF-HSR	48.9073	1.3078	1.3065	0.9911

5.4 HSR with AGK

We use the Houston2013 dataset to evaluate HSR performance under AGK spatial blurring. In order to exam the impact of the blurring kernel's rank on fusion results, we spatially degenerate each SRI using four different AGKs of the size 9×9 , each with a different condition number, then downsample the blurred images by a factor of 8 to obtain four $32 \times 32 \times 144$ HSIs. The four AGKs are depicted in Fig. 7 and will be referred to as AGK 1–4 hereafter.

Results for non-blind experiments with AGK 1–4 are presented in Figs. 8 and 9 as well as Tables 2–5. The most

TABLE 4: Performance on the Houston2013 dataset with AGK 3 (averaged over 20 scenes)

Setup	Methods	Quality Indices			
		PSNR \uparrow	RMSE \downarrow	SAM \downarrow	SSIM \uparrow
Non-blind	Hysure	40.9898	2.5609	2.3835	0.9779
	SURE	45.7364	1.4738	1.4674	0.9885
	LTMR	48.4784	1.3547	1.3286	0.9901
	LRTA	45.1557	2.4806	2.3766	0.9753
	ZSL	46.4985	1.4322	1.4222	0.9918
	STEREO	38.2735	4.6097	4.2564	0.9429
	CSTF	37.8331	3.7743	2.6188	0.9733
	FSTRD	38.5440	4.0143	3.5216	0.9406
	BGS-GTF-HSR	49.1722	1.2147	1.2538	0.9917
Blind	Hysure	40.2239	2.8393	2.6308	0.9756
	SURE	45.7367	1.4738	1.4674	0.9885
	LTMR	47.7609	1.4880	1.3899	0.9893
	LRTA	45.3971	2.3589	2.1870	0.9786
	ZSL	46.4985	1.4322	1.4222	0.9910
	B-STE	44.1948	2.0406	2.2681	0.9757
	CSTF	41.6336	2.4721	2.0977	0.9830
	FSTRD	40.4948	3.1464	3.0553	0.9566
	BGS-GTF-HSR	48.9543	1.2798	1.2898	0.9913

TABLE 5: Performance on the Houston2013 dataset with AGK 4 (averaged over 20 scenes)

Setup	Methods	Quality Indices			
		PSNR \uparrow	RMSE \downarrow	SAM \downarrow	SSIM \uparrow
Non-blind	Hysure	40.6767	2.6430	2.3746	0.9757
	SURE	45.9881	1.4210	1.4318	0.9894
	LTMR	48.5138	1.3441	1.3206	0.9903
	LRTA	43.9408	3.1656	2.9178	0.9657
	ZSL	46.6561	1.4023	1.3884	0.9917
	STEREO	34.2605	7.7812	6.7030	0.9104
	CSTF	33.1642	6.0793	3.6365	0.9313
	FSTRD	34.8040	6.1536	4.7125	0.9042
	BGS-GTF-HSR	49.1804	1.2131	1.2524	0.9919
Blind	Hysure	39.9899	2.9175	2.6524	0.9742
	SURE	45.9881	1.4210	1.4318	0.9894
	LTMR	47.8431	1.4443	1.3709	0.9895
	LRTA	45.4547	2.3440	2.1988	0.9783
	ZSL	46.6561	1.4023	1.3884	0.9914
	B-STE	44.1122	2.0621	2.2928	0.9752
	CSTF	40.5917	2.7768	2.2238	0.9798
	FSTRD	39.5407	3.5931	3.5120	0.9436
	BGS-GTF-HSR	49.0451	1.2468	1.2685	0.9916

salient phenomenon in the visual results is the systematic failure of the TF-based STEREO, CSTF, and FSTRD under anisotropic blurring. Since the AGK is not rank 1, the assumptions underlying the TF framework deviate from the real spatial degradation, resulting in dramatically degraded performance relative to the MF- and GTF-based approaches. A similar conclusion can be drawn from the quantitative results in Tables 2–5. Additionally, Fig. 10 depicts how performance changes as the rank of the AGK increases. We see that the MF-based techniques along with the proposed BGS-GTF-HSR are largely resilient to increasing rank, whereas

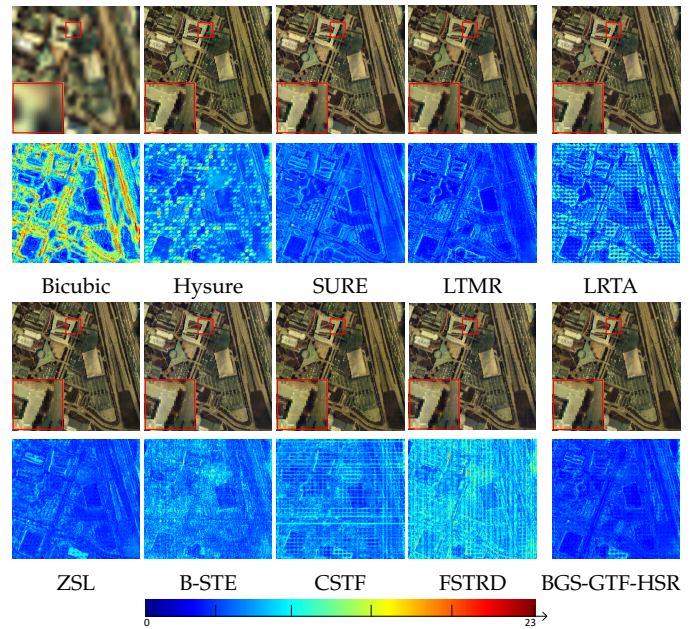


Fig. 11: Blind fusion results and error maps for the Houston2013 dataset with AGK 3 (Scene 17). Pseudo-color is composed of bands 30, 20 and 10.

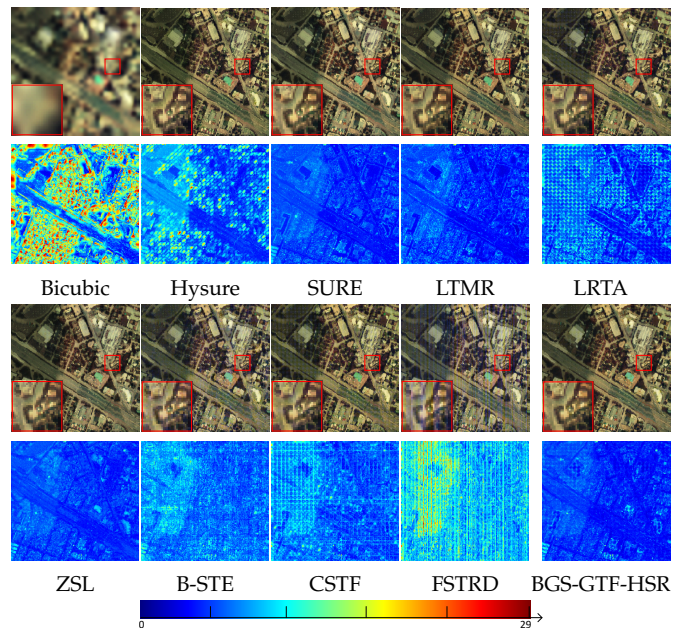


Fig. 12: Blind fusion results and error maps for the Houston2013 dataset with AGK 4 (Scene 5). Pseudo-color is composed of bands 30, 20 and 10.

the TF-based techniques suffer greatly.

The results for blind experiments are presented in Figs. 11 and 12 as well as in Tables 2–5. Again, the TF-based methods largely fail to adequately handle the anisotropic blurring. Interestingly, however, the TF-based methods do better in the blind experiments than they do in the non-blind experiments, particularly for AGK 3 and AGK 4. While this appears counter-intuitive, these results imply that the spatial-degradation matrices used in TF-based fusions do

not necessarily have to match the real degradation. Nevertheless, the proposed BGS-GTF-HSR consistently outperforms all the other techniques for the blind-fusion scenario.

5.5 HSR on a Real Dataset

The fusion results are depicted in Fig. 13 as pseudo-color images for the real Houston2018 HSI/MSI pair. Since there exists no ground truth, we can compare only the visual results from the perspectives of spatial enhancement and spectral fidelity. On the one hand, one can observe strong artifacts from the zoomed-in areas in Fig. 13 for Hysure, LTM, LRTA, CSTF, and FSTRD, yet, such artifacts are much less obvious for BGS-GTF-HSR. If, on the other hand, the pseudo-color results of ZSL and B-STE appear finer and smoother, it is only because they have actually overfit the spatial information of the MSI but failed to maintain the spectral information of the HSI. To show this, we graph some spectral-pixel curves in Fig. 14 and see that the curves for ZSL and B-STE severely deviate from those of the HSI whereas the curves for BGS-GTF-HSR are much closer to their HSI counterparts.

6 CONCLUSION

In this paper, we proposed a generalization of the TF-based HSR problem in the form of GTF-HSR. We demonstrated that this generalization can model arbitrary forms of blurring kernels, whereas previous TF-HSR approaches cannot handle situations wherein the blurring kernel was not rank-1. We also addressed the recoverability of the proposed GTF-HSR, showing that exact recovery is guaranteed. To establish an algorithmic framework for practical HSR, we proposed a blockwise-sparse regularizer to fully exploit the group sparsity of higher-order tensors, which is achieved through a block-based unfolding strategy and the $l_{2,0}$ -norm. With the nonconvex surrogate imposed, the overall problem was optimized via ADMM in a divide-and-conquer manner to ease the intrinsic difficulty of large-scale nonconvex optimization for multi-source data reconstruction. We tested our proposed algorithmic framework, called BGS-GTF-HSR, on simulated datasets under traditional isotropic Gaussian blurring as well as more realistic anisotropic Gaussian blurring and also on real HSI-MSI pairs. Experimental results demonstrated that our proposed BGS-GTF-HSR outperformed the TF-HSR methods considered under anisotropic blurring in simulated problems for both blind as well as non-blind HSR. Additionally, superior results were observed for BGS-GTF-HSR for real-world data as well.

7 SUPPLEMENTAL MATERIAL

7.1 Proofs of Propositions, Lemmas, Theorems, and Corollaries in the Paper

In this section, we provided detailed proofs of propositions, lemmas, theorems, and corollaries found in the main text. In this supplemental material, \mathbf{A}^\dagger represents the Moore-Penrose pseudo-inverse of \mathbf{A} , and \oplus denotes the direct sum of two spaces. For a 3-way tensor $\mathcal{T} \in \mathbb{R}^{M \times N \times L}$, $\mathbf{T}_{M \times N, l}$ denotes its l^{th} frontal slice, and $\mathcal{T}[m, n, :]$ denotes its pixel vector at spatial location (m, n) . Furthermore, $\mathbf{T}[m, n]$ denotes the (m, n) element of matrix \mathbf{T} , $\mathbf{t}[m]$ denotes the m^{th}

element of vector \mathbf{t} , and \mathbf{t}_m denotes the m^{th} column vector of matrix \mathbf{T} . We use \mathbf{I}_N and \mathbf{L}_N to indicate the $N \times N$ identity and commutation matrices, respectively. Finally, $P(\cdot)$ stands for the probability function.

7.2 Proof of Prop. 3.1

In proving Prop. 3.1, we first introduce Lemma 7.1 followed by Corollary 7.1.

Lemma 7.1. *For arbitrary matrices $\mathbf{M}_1 \in \mathbb{R}^{J_1 \times K_1}$ and $\mathbf{M}_2 \in \mathbb{R}^{J_2 \times K_2}$, there exists a reversible linear mapping $F(\cdot|J_1, J_2, K_1, K_2)$, such that*

$$\mathbf{M}_1 \otimes \mathbf{M}_2 = F\left(\text{Vec}(\mathbf{M}_1) \text{Vec}^T(\mathbf{M}_2) | J_1, J_2, K_1, K_2\right) \quad (7.1)$$

and

$$\text{Vec}(\mathbf{M}_1) \text{Vec}^T(\mathbf{M}_2) = F^{-1}\left(\mathbf{M}_1 \otimes \mathbf{M}_2 | J_1, J_2, K_1, K_2\right) \quad (7.2)$$

where

$$\begin{aligned} F(\cdot|J_1, J_2, K_1, K_2) &= \\ \text{Unv}\left[\left(\mathbf{I}_{K_1} \otimes \mathbf{L}_{K_2 J_1} \otimes \mathbf{I}_{J_2}\right) \text{Vec}\left(\left(\cdot\right)^T\right) | J_1 J_2, K_1 K_2\right], \\ F^{-1}(\cdot|J_1, J_2, K_1, K_2) &= \\ \text{Unv}^T\left[\left(\mathbf{I}_{K_1} \otimes \mathbf{L}_{J_1 K_2} \otimes \mathbf{I}_{J_2}\right) \text{Vec}(\cdot) | J_1 K_1, J_2 K_2\right]. \end{aligned} \quad (7.3)$$

Proof. One can see the existence of this map and its reversibility by verifying that

$$\begin{aligned} \text{Vec}(\mathbf{M}_1 \otimes \mathbf{M}_2) &= \\ &= \left(\mathbf{I}_{K_1} \otimes \mathbf{L}_{K_2 J_1} \otimes \mathbf{I}_{J_2}\right) \left(\text{Vec}(\mathbf{M}_1) \otimes \text{Vec}(\mathbf{M}_2)\right) \\ &= \left(\mathbf{I}_{K_1} \otimes \mathbf{L}_{K_2 J_1} \otimes \mathbf{I}_{J_2}\right) \text{Vec}\left(\text{Vec}(\mathbf{M}_2) \text{Vec}^T(\mathbf{M}_1)\right), \end{aligned} \quad (7.4)$$

and its linearity simply follows from the linearity of $\text{Vec}(\cdot)$, $\text{Unv}(\cdot)$, and matrix multiplication. \square

Corollary 7.1. *For any matrix $\mathbf{W} \in \mathbb{R}^{J_1 J_2 \times K_1 K_2}$, its Kronecker rank is as*

$$\text{kr}_{\mathbf{W}} = \text{rank}\left\{F^{-1}\left(\mathbf{W} | J_1, J_2, K_1, K_2\right)\right\}. \quad (7.5)$$

Proof. Letting $R = \text{rank}\left\{F^{-1}\left(\mathbf{W} | J_1, J_2, K_1, K_2\right)\right\}$, there exist $\mathbf{A} \in \mathbb{R}^{J_1 K_1 \times R}$ and $\mathbf{B} \in \mathbb{R}^{J_2 K_2 \times R}$ such that

$$F^{-1}\left(\mathbf{W} | J_1, J_2, K_1, K_2\right) = \mathbf{A} \mathbf{B}^T. \quad (7.6)$$

Let $\mathbf{M}_1^{(r)} = \text{Unv}\left(\mathbf{a}_r | J_1, K_1\right)$ and $\mathbf{M}_2^{(r)} = \text{Unv}\left(\mathbf{b}_r | J_2, K_2\right)$, where \mathbf{a}_r and \mathbf{b}_r are the r^{th} columns of matrices \mathbf{A} and \mathbf{B} , respectively. We then have

$$\begin{aligned} \mathbf{W} &= F\left(F^{-1}\left(\mathbf{W} | J_1, J_2, K_1, K_2\right) | J_1, J_2, K_1, K_2\right) \\ &= F\left(\mathbf{A} \mathbf{B}^T | J_1, J_2, K_1, K_2\right) \\ &= F\left(\sum_{r=1}^R \mathbf{a}_r \mathbf{b}_r^T | J_1, J_2, K_1, K_2\right) \\ &= \sum_{r=1}^R F\left(\mathbf{a}_r \mathbf{b}_r^T | J_1, J_2, K_1, K_2\right) \end{aligned}$$

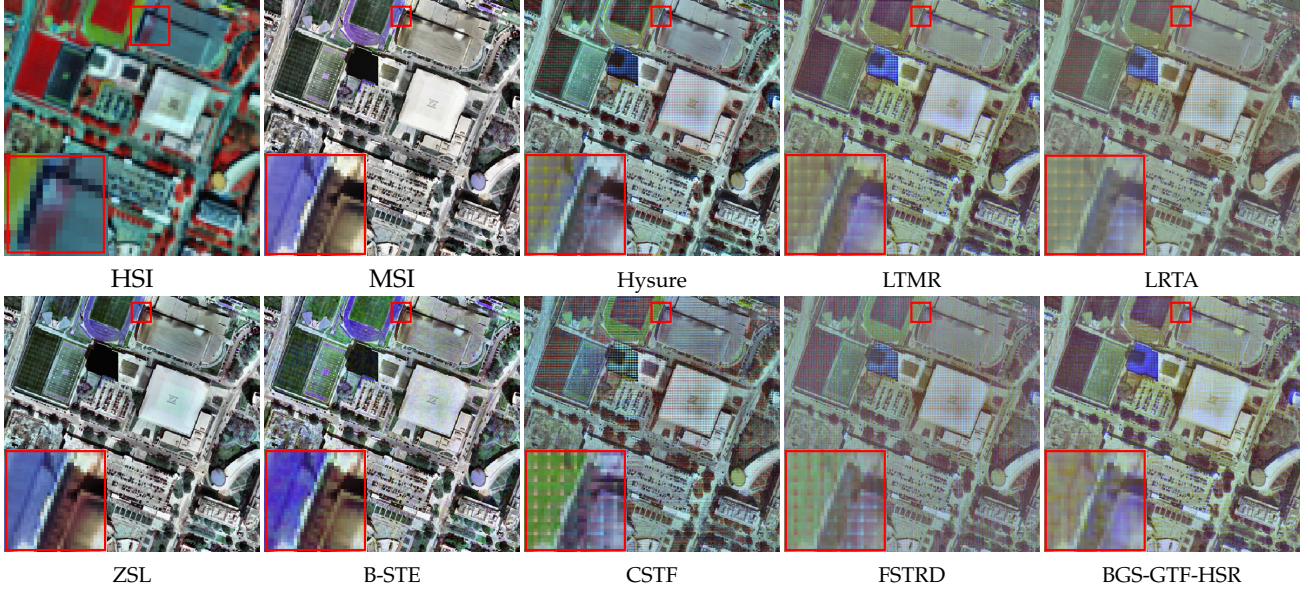


Fig. 13: Fusion results on the Houston2018 dataset; pseudo-color is composed of bands 30, 20 and 10.

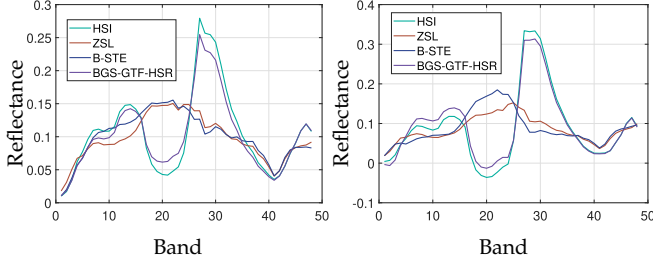


Fig. 14: Two spectral curves from the Houston2018 dataset.

$$= \sum_{r=1}^R \mathbf{M}_1^{(r)} \otimes \mathbf{M}_2^{(r)}, \quad (7.7)$$

which implies that $\text{kr}_{\mathbf{W}} \leq \text{rank} \{ \mathbf{F}^{-1}(\mathbf{W}|_{J_1, J_2, K_1, K_2}) \}$. On the other hand, supposing the “tightest” KD of \mathbf{W} is $\mathbf{W} = \sum_{r=1}^{\text{kr}_{\mathbf{W}}} \mathbf{M}_1^{(r)} \otimes \mathbf{M}_2^{(r)}$, we then have

$$\begin{aligned} & \mathbf{F}^{-1}(\mathbf{W}|_{J_1, J_2, K_1, K_2}) \\ &= \mathbf{F}^{-1} \left(\sum_{r=1}^{\text{kr}_{\mathbf{W}}} \mathbf{M}_1^{(r)} \otimes \mathbf{M}_2^{(r)} \Big|_{J_1, J_2, K_1, K_2} \right) \\ &= \sum_{r=1}^{\text{kr}_{\mathbf{W}}} \mathbf{F}^{-1}(\mathbf{M}_1^{(r)} \otimes \mathbf{M}_2^{(r)} \Big|_{J_1, J_2, K_1, K_2}) \\ &= \sum_{r=1}^{\text{kr}_{\mathbf{W}}} \text{Vec} \left(\mathbf{M}_1^{(r)} \right) \text{Vec}^T \left(\mathbf{M}_2^{(r)} \right) \end{aligned} \quad (7.8)$$

which implies that $\text{kr}_{\mathbf{W}} \geq \text{rank} \{ \mathbf{F}^{-1}(\mathbf{W}|_{J_1, J_2, K_1, K_2}) \}$. Thus, it is proven that $\text{kr}_{\mathbf{W}} = \text{rank} \{ \mathbf{F}^{-1}(\mathbf{W}|_{J_1, J_2, K_1, K_2}) \}$. \square

Next, we start to prove Prop. 3.1. We first derive the explicit expression of spatial-degradation matrix \mathbf{D} then complete the proof by taking Cor. 7.1 into account.

Proposition 3.1. For the spatial-degradation matrix \mathbf{D} in (2.5), since it is physically modeled as (3.2), we have

$$\text{kr}_{\mathbf{D}} = \text{rank} \{ \Phi \}. \quad (7.9)$$

Proof. To prove Prop. 3.1, we give an explicit expression of \mathbf{D} in terms of the blurring kernel Φ and the specific down-sampling strategy. First, suppose the rank decomposition of Φ is

$$\Phi = \mathbf{U}\mathbf{V}^T = \sum_{r=1}^R \mathbf{u}_r \mathbf{v}_r^T, \quad (7.10)$$

where $\mathbf{U}, \mathbf{V} \subseteq \mathbb{R}^{\phi \times R}$ are matrices with full column rank, and $R = \text{rank} \{ \Phi \}$. Then, let \mathbf{u}_r and \mathbf{v}_r be the r^{th} column vectors of \mathbf{U} and \mathbf{V} , respectively. Subsequently, defining $\tilde{\mathbf{Z}} = \mathbf{Z} * \Phi$, we have

$$\begin{aligned} \tilde{\mathbf{Z}}[m, n, :] &= \sum_{l, s=1}^{\phi, \phi} \Phi[l, s] \mathbf{Z}[m - m' + l, n - n' + s, :] \\ &= \sum_{l, s=1}^{\phi, \phi} \sum_{r=1}^R \mathbf{u}_r[l] \mathbf{v}_r[s] \mathbf{Z}[m - m' + l, n - n' + s, :] \\ &= \sum_{r=1}^R \sum_{l, s=1}^{\phi, \phi} \mathbf{u}_r[l] \mathbf{Z}[m - m' + l, n - n' + s, :] \mathbf{v}_r[s], \end{aligned} \quad (7.11)$$

where m', n' are the shift parameters [28]. This actually implies that

$$\tilde{\mathbf{Z}} = \mathbf{Z} * \Phi = \sum_{r=1}^R \mathbf{Z} * \mathbf{u}_r * \mathbf{v}_r^T = \sum_{r=1}^R \mathbf{Z} \times_1 \mathbf{T}^{\mathbf{u}_r} \times_2 \mathbf{T}^{\mathbf{v}_r}, \quad (7.12)$$

in which $\{ \mathbf{T}^{\mathbf{u}_r}, \mathbf{T}^{\mathbf{v}_r} \}_{r=1}^R$ are circulant matrices generated according to $\{ \mathbf{u}_r, \mathbf{v}_r \}_{r=1}^R$. More concretely,

$$\mathbf{T}^{\mathbf{u}_r} = \sum_{l=1}^{\phi} \mathbf{u}_r[l] \mathbf{J}_{M_1}^{M_1 - m' + l}, \quad (7.13)$$

$$\mathbf{T}^{\mathbf{v}_r} = \sum_{s=1}^{\phi} \mathbf{v}_r[s] \mathbf{J}_{M_2}^{M_2 - n' + s}, \quad (7.14)$$

and \mathbf{J}_M denotes the $M \times M$ basic circulant matrix,

$$\mathbf{J}_M = \begin{bmatrix} 0 & 1 & 0 & \cdots & 0 \\ 0 & 0 & 1 & \cdots & 0 \\ \vdots & \vdots & \vdots & \ddots & \vdots \\ 0 & 0 & 0 & \cdots & 1 \\ 1 & 0 & 0 & \cdots & 0 \end{bmatrix}. \quad (7.15)$$

Having expressed the blurring aspect of the spatial degradation, we now consider the subsequent uniform down-sampling, yielding an expression for the whole spatial-degradation process,

$$\mathcal{X} = (\mathcal{Z} * \Phi)_{\downarrow} = \sum_{r=1}^R \mathcal{Z} \times_1 \mathbf{P}_1^{(r)} \times_2 \mathbf{P}_2^{(r)}, \quad (7.16)$$

where

$$\mathbf{P}_1^{(r)} = \mathbf{S}_1 \mathbf{T}^{\mathbf{u}_r}, \quad (7.17)$$

$$\mathbf{P}_2^{(r)} = \mathbf{S}_2 \mathbf{T}^{\mathbf{v}_r}, \quad (7.18)$$

and the row vectors of $\mathbf{S}_1 \in \mathbb{R}^{m_1 \times M_1}$ and $\mathbf{S}_2 \in \mathbb{R}^{m_2 \times M_2}$ are sampled from those of \mathbf{I}_{M_1} and \mathbf{I}_{M_2} , respectively. Combining with (3.2), we now have

$$\mathbf{X}_{[3]} = \mathbf{Z}_{[3]} \mathbf{D} = \mathbf{Z}_{[3]} \sum_{r=1}^R \left(\mathbf{P}_2^{(r)} \otimes \mathbf{P}_1^{(r)} \right)^T. \quad (7.19)$$

Since this equation should hold for any \mathcal{Z} , it is concluded that

$$\mathbf{D} = \sum_{r=1}^R \left(\mathbf{P}_2^{(r)} \otimes \mathbf{P}_1^{(r)} \right)^T. \quad (7.20)$$

To proceed, from Cor. 7.1, we have

$$\begin{aligned} \text{kr}_{\mathbf{D}} &= \text{rank} \left\{ \mathbf{F}^{-1}(\mathbf{D} | M_2, M_1, m_2, m_1) \right\} \\ &= \text{rank} \left\{ \mathbf{F}^{-1} \left(\sum_{r=1}^R \left(\mathbf{P}_2^{(r)} \otimes \mathbf{P}_1^{(r)} \right)^T \mid M_2, M_1, m_2, m_1 \right) \right\} \\ &= \text{rank} \left\{ \sum_{r=1}^R \text{Vec} \left(\left(\mathbf{P}_2^{(r)} \right)^T \right) \text{Vec}^T \left(\left(\mathbf{P}_1^{(r)} \right)^T \right) \right\}. \end{aligned} \quad (7.21)$$

Denoting $\{\mathbf{q}_j^{(r)}\}_{j=1}^{m_2}$ and $\{\mathbf{p}_i^{(r)}\}_{i=1}^{m_1}$ to be the column vectors of $(\mathbf{P}_2^{(r)})^T$ and $(\mathbf{P}_1^{(r)})^T$, respectively, we can further derive that

$$\begin{aligned} & \sum_{r=1}^R \text{Vec} \left(\left(\mathbf{P}_2^{(r)} \right)^T \right) \text{Vec}^T \left(\left(\mathbf{P}_1^{(r)} \right)^T \right) \\ &= \sum_{r=1}^R \begin{bmatrix} \mathbf{q}_1^{(r)} \\ \mathbf{q}_2^{(r)} \\ \vdots \\ \mathbf{q}_{m_2}^{(r)} \end{bmatrix} \begin{bmatrix} \mathbf{p}_1^{(r)T} & \mathbf{p}_2^{(r)T} & \cdots & \mathbf{p}_{m_1}^{(r)T} \end{bmatrix}. \end{aligned} \quad (7.22)$$

Due to the fact that $\{\mathbf{q}_j^{(r)T}\}_{j=1}^{m_2}$ and $\{\mathbf{p}_i^{(r)T}\}_{i=1}^{m_1}$ are all sampled from the rows of circulant matrices, we further have

$$\begin{aligned} & \text{rank} \left\{ \sum_{r=1}^R \begin{bmatrix} \mathbf{q}_1^{(r)} \\ \mathbf{q}_2^{(r)} \\ \vdots \\ \mathbf{q}_{m_2}^{(r)} \end{bmatrix} \begin{bmatrix} \mathbf{p}_1^{(r)T} & \mathbf{p}_2^{(r)T} & \cdots & \mathbf{p}_{m_1}^{(r)T} \end{bmatrix} \right\} \\ &= \text{rank} \left\{ \sum_{r=1}^R \begin{bmatrix} \mathbf{q}_1^{(r)} \\ \mathbf{q}_2^{(r)} \\ \vdots \\ \mathbf{q}_{m_2}^{(r)} \end{bmatrix} \begin{bmatrix} \mathbf{p}_1^{(r)T} & \mathbf{p}_2^{(r)T} & \cdots & \mathbf{p}_{m_1}^{(r)T} \end{bmatrix} \right\} \\ &= \text{rank} \left\{ \sum_{r=1}^R \mathbf{q}_1^{(r)} \mathbf{p}_1^{(r)T} \right\} \\ &= \text{rank} \left\{ \sum_{r=1}^R \mathbf{v}_r \mathbf{u}_r^T \right\} \\ &= \text{rank} \{ \Phi \}, \end{aligned} \quad (7.23)$$

which completes the proof. \square

7.3 Proof of Thm. 3.2

To prove Thm. 3.2, we first introduce the following lemma.

Lemma 7.2. *Let an arbitrary three-way tensor $\mathcal{T} \in \mathbb{R}^{M \times N \times L}$ be decomposed as*

$$\mathcal{T} = \sum_{r=1}^R \mathcal{C} \times_1 \mathbf{A}_r \times_2 \mathbf{B}_r, \quad (7.24)$$

where $\mathcal{C} \in \mathbb{R}^{I \times J \times L}$ is drawn from an absolutely continuous distribution, and $\mathbf{A}_r \in \mathbb{R}^{M \times I}$ and $\mathbf{B}_r \in \mathbb{R}^{N \times J}$. Suppose that

$$\begin{aligned} I &\leq JL, \quad J \leq IL, \quad L \geq 3, \\ \text{rank} \{ \mathbf{A} \} &= IR, \\ \text{rank} \{ \mathbf{B} \} &= JR, \end{aligned} \quad (7.25)$$

where

$$\begin{aligned} \mathbf{A} &= [\mathbf{A}_1, \mathbf{A}_2, \cdots, \mathbf{A}_R], \\ \mathbf{B} &= [\mathbf{B}_1, \mathbf{B}_2, \cdots, \mathbf{B}_R]. \end{aligned} \quad (7.26)$$

Then this decomposition of \mathcal{T} in terms of \mathcal{C} , \mathbf{A} , and \mathbf{B} is essentially unique with probability 1.

Remark 7.1. *Here, essential uniqueness means that we can find alternative $\hat{\mathcal{C}} \in \mathbb{R}^{I \times J \times L}$, $\hat{\mathbf{A}}_r \in \mathbb{R}^{M \times I}$, and $\hat{\mathbf{B}}_r \in \mathbb{R}^{N \times J}$ such that*

$$\mathcal{T} = \sum_{r=1}^R \hat{\mathcal{C}} \times_1 \hat{\mathbf{A}}_r \times_2 \hat{\mathbf{B}}_r, \quad (7.27)$$

only if

$$\hat{\mathbf{A}}_r = \mathbf{A}_r \Psi_{\mathbf{A}}^{(r)}, \quad (7.28)$$

$$\hat{\mathbf{B}}_r = \mathbf{B}_r \Psi_{\mathbf{B}}^{(r)}, \quad (7.29)$$

and

$$\hat{\mathcal{C}} = \mathcal{C} \times_1 \left(\Psi_{\mathbf{A}}^{(r)} \right)^{-1} \times_2 \left(\Psi_{\mathbf{B}}^{(r)} \right)^{-1}, \quad (7.30)$$

where $\Psi_{\mathbf{A}}^{(r)} \in \mathbb{R}^{I \times I}$, and $\Psi_{\mathbf{B}}^{(r)} \in \mathbb{R}^{J \times J}$ are nonsingular matrices. We note that Lemma 7.2 can be considered to be a variant of Theorem 6.1 in [43]. However, the different supposition made

here on the genericity of \mathcal{C} requires a separate proof, which we present now.

Proof. To begin, it is easy to verify that

$$\mathbf{T}_{M \times N, 2} \mathbf{T}_{M \times N, 1}^\dagger = \mathbf{A}(\mathbf{I}_R \otimes \mathbf{C}_{I \times J, 2} \mathbf{C}_{I \times J, 1}^\dagger) \mathbf{A}^\dagger, \quad (7.31)$$

$$\mathbf{T}_{M \times N, 3} \mathbf{T}_{M \times N, 1}^\dagger = \mathbf{A}(\mathbf{I}_R \otimes \mathbf{C}_{I \times J, 3} \mathbf{C}_{I \times J, 1}^\dagger) \mathbf{A}^\dagger. \quad (7.32)$$

Subtracting these two equations, we obtain

$$\mathbf{E}_{\mathcal{T}} \triangleq (\mathbf{T}_{M \times N, 3} - \mathbf{T}_{M \times N, 2}) \mathbf{T}_{M \times N, 1}^\dagger = \mathbf{A}(\mathbf{I}_R \otimes \mathbf{E}_{\mathcal{C}}) \mathbf{A}^\dagger, \quad (7.33)$$

where $\mathbf{E}_{\mathcal{C}} \triangleq (\mathbf{C}_{M \times N, 3} - \mathbf{C}_{M \times N, 2}) \mathbf{C}_{M \times N, 1}^\dagger$. Benefiting from the genericity of \mathcal{C} , $\mathbf{E}_{\mathcal{C}}$ is also generic. Moreover, it is implied that the column space of each \mathbf{A}_r is an invariant subspace of $\mathbf{E}_{\mathcal{T}}$, which means that

$$\text{col}\{\mathbf{E}_{\mathcal{T}}\} = \text{col}\{\mathbf{A}_1\} \oplus \text{col}\{\mathbf{A}_2\} \oplus \cdots \oplus \text{col}\{\mathbf{A}_R\}. \quad (7.34)$$

Now, if \mathcal{T} can be alternatively decomposed into

$$\mathcal{T} = \sum_{r=1}^R \hat{\mathbf{C}} \times_1 \hat{\mathbf{A}}_r \times_2 \hat{\mathbf{B}}_r, \quad (7.35)$$

where $\hat{\mathbf{C}} \in \mathbb{R}^{I \times J \times L}$, $\hat{\mathbf{A}}_r \in \mathbb{R}^{M \times I}$, and $\hat{\mathbf{B}}_r \in \mathbb{R}^{N \times J}$, we could similarly derive that

$$\text{col}\{\mathbf{E}_{\mathcal{T}}\} = \text{col}\{\hat{\mathbf{A}}_1\} \oplus \text{col}\{\hat{\mathbf{A}}_2\} \oplus \cdots \oplus \text{col}\{\hat{\mathbf{A}}_R\}. \quad (7.36)$$

Denoting $V_{\hat{r}}^{(r)}$ to indicate the number of columns in $\hat{\mathbf{A}}_r$ that belong to $\text{col}\{\hat{\mathbf{A}}_{\hat{r}}\}$, $\hat{r} = 1, 2, \dots, R$, we have that $V_{\hat{r}}^{(r)} \geq 0$, and $\sum_{\hat{r}=1}^R V_{\hat{r}}^{(r)} = I$. If $\max_{\hat{r}} \{V_{\hat{r}}^{(r)}\} < I$, then, because $\text{col}\{\hat{\mathbf{A}}_{\hat{r}_1}\} \cap \text{col}\{\hat{\mathbf{A}}_{\hat{r}_2}\} = \emptyset$, $\forall \hat{r}_1 \neq \hat{r}_2$, it can be concluded that there exists at least one zero element in each column of $\mathbf{E}_{\mathcal{C}}$ since

$$\mathbf{E}_{\mathcal{T}} \mathbf{A}_r = \mathbf{A}_r \mathbf{E}_{\mathcal{C}}. \quad (7.37)$$

Thus $\|\mathbf{E}_{\mathcal{C}}\|_0 \leq I^2 - I$, and there exist finite mappings to rearrange the elements of $\mathbf{E}_{\mathcal{C}}$ to get $\mathbf{E}'_{\mathcal{C}}$ whose last row is all zero. However, due to the genericity of $\mathbf{E}_{\mathcal{C}}$, $\mathbf{E}'_{\mathcal{C}}$ is also generic. Thus, based on Prop. 2.7 in [57],

$$\mathbb{P}\left(\text{rank}\{\mathbf{E}'_{\mathcal{C}}\} \leq \|(\mathbf{E}'_{\mathcal{C}})^T\|_{2,0} < I\right) = 0. \quad (7.38)$$

Therefore, we are able to conclude that, with probability 1,

$$\max_{\hat{r}} \{V_{\hat{r}}^{(r)}\} = I, \quad (7.39)$$

which implies that, $\forall \hat{r}, \exists r_{\hat{r}} \in \{1, 2, \dots, R\}$ such that

$$\text{col}\{\hat{\mathbf{A}}_{\hat{r}}\} = \text{col}\{\mathbf{A}_{r_{\hat{r}}}\}, \quad (7.40)$$

and, $\forall \hat{r}_1 \neq \hat{r}_2$, we have $r_{\hat{r}_1} \neq r_{\hat{r}_2}$. Without loss of generality, suppose $\text{col}\{\hat{\mathbf{A}}_{\hat{r}}\} = \text{col}\{\mathbf{A}_{r_{\hat{r}}}\}$, $\forall r \in \{1, 2, \dots, R\}$ (or we could permute the order of $\{\hat{\mathbf{A}}_{\hat{r}}\}_{\hat{r}=1}^R$ to have this be true). Then it follows that

$$\hat{\mathbf{A}}_r = \mathbf{A}_r \Psi_{\mathbf{A}}^{(r)}, \quad (7.41)$$

where $\Psi_{\mathbf{A}}^{(r)} \in \mathbb{R}^{I \times I}$ is some nonsingular matrix.

Applying the same analysis above on the second dimension of \mathcal{T} , it can be deduced that, with probability 1, $\forall \hat{r}$,

there exist $r_{\hat{r}} \in \{1, 2, \dots, R\}$ and nonsingular $\Psi_{\mathbf{B}}^{(\hat{r})} \in \mathbb{R}^{J \times J}$ such that

$$\hat{\mathbf{B}}_{\hat{r}} = \mathbf{B}_{r_{\hat{r}}} \Psi_{\mathbf{B}}^{(\hat{r})}. \quad (7.42)$$

Consequently, we have

$$\begin{aligned} \mathcal{T} &= \sum_{\hat{r}=1}^R \hat{\mathbf{C}} \times_1 \hat{\mathbf{A}}_{\hat{r}} \times_2 \hat{\mathbf{B}}_{\hat{r}} \\ &= \sum_{\hat{r}=1}^R \hat{\mathbf{C}} \times_1 \mathbf{A}_{r_{\hat{r}}} \Psi_{\mathbf{A}}^{(\hat{r})} \times_2 \mathbf{B}_{r_{\hat{r}}} \Psi_{\mathbf{B}}^{(\hat{r})} \\ &= \sum_{\hat{r}=1}^R \hat{\mathcal{C}}^{(\hat{r})} \times_1 \mathbf{A}_{\hat{r}} \times_2 \mathbf{B}_{r_{\hat{r}}}, \end{aligned} \quad (7.43)$$

where $\hat{\mathcal{C}}^{(\hat{r})} \triangleq \hat{\mathbf{C}} \times_1 \Psi_{\mathbf{A}}^{(\hat{r})} \times_2 \Psi_{\mathbf{B}}^{(\hat{r})}$. Performing mode-2 unfolding, we further have

$$\begin{aligned} \mathbf{T}_{[2]} &= [\mathbf{B}_1 \quad \mathbf{B}_2 \quad \cdots \quad \mathbf{B}_R] \begin{bmatrix} \mathbf{C}_{[2]} & & & \\ & \mathbf{C}_{[2]} & & \\ & & \ddots & \\ & & & \mathbf{C}_{[2]} \end{bmatrix} \\ &\quad \times (\mathbf{I}_{LR} \otimes \mathbf{A})^T \\ &= [\mathbf{B}_{r_1} \quad \mathbf{B}_{r_2} \quad \cdots \quad \mathbf{B}_{r_R}] \begin{bmatrix} \hat{\mathbf{C}}_{[2]}^{(1)} & & & \\ & \hat{\mathbf{C}}_{[2]}^{(2)} & & \\ & & \ddots & \\ & & & \hat{\mathbf{C}}_{[2]}^{(R)} \end{bmatrix} \\ &\quad \times (\mathbf{I}_{LR} \otimes \mathbf{A})^T \\ &= [\mathbf{B}_1 \quad \mathbf{B}_2 \quad \cdots \quad \mathbf{B}_R] \mathbf{\Pi}_{\mathbf{B}} \begin{bmatrix} \hat{\mathbf{C}}_{[2]}^{(1)} & & & \\ & \hat{\mathbf{C}}_{[2]}^{(2)} & & \\ & & \ddots & \\ & & & \hat{\mathbf{C}}_{[2]}^{(R)} \end{bmatrix} \\ &\quad \times (\mathbf{I}_{LR} \otimes \mathbf{A})^T, \end{aligned} \quad (7.44)$$

where $\mathbf{\Pi}_{\mathbf{B}} \in \mathbb{R}^{JR \times JR}$ is a block permutation matrix. Because $[\mathbf{B}_1 \quad \mathbf{B}_2 \quad \cdots \quad \mathbf{B}_R]$ has full column rank, and $(\mathbf{I}_{LR} \otimes \mathbf{A})^T$ is of full row rank, we have that

$$\begin{bmatrix} \mathbf{C}_{[2]} & & & \\ & \mathbf{C}_{[2]} & & \\ & & \ddots & \\ & & & \mathbf{C}_{[2]} \end{bmatrix} = \mathbf{\Pi}_{\mathbf{B}} \begin{bmatrix} \hat{\mathbf{C}}_{[2]}^{(1)} & & & \\ & \hat{\mathbf{C}}_{[2]}^{(2)} & & \\ & & \ddots & \\ & & & \hat{\mathbf{C}}_{[2]}^{(R)} \end{bmatrix}. \quad (7.45)$$

Thus, $\mathbf{\Pi}_{\mathbf{B}}$ block-wisely permutes a block diagonal matrix into another block diagonal matrix, which happens if and only if

$$\mathbf{\Pi}_{\mathbf{B}} = \mathbf{I}_{JR}. \quad (7.46)$$

It then follows directly that $r_{\hat{r}} = \hat{r}$, and, more importantly,

$$\begin{aligned} \hat{\mathbf{A}}_1 &= \mathbf{A}_1 \Psi_{\mathbf{A}}^{(1)}, \\ \hat{\mathbf{A}}_2 &= \mathbf{A}_2 \Psi_{\mathbf{A}}^{(2)}, \\ &\vdots \\ \hat{\mathbf{A}}_R &= \mathbf{A}_R \Psi_{\mathbf{A}}^{(R)}, \end{aligned} \quad (7.47)$$

$$\begin{aligned}
\hat{\mathbf{B}}_1 &= \mathbf{B}_1 \Psi_{\mathbf{B}}^{(1)}, \\
\hat{\mathbf{B}}_2 &= \mathbf{B}_2 \Psi_{\mathbf{B}}^{(2)}, \\
&\vdots \\
\hat{\mathbf{B}}_R &= \mathbf{B}_R \Psi_{\mathbf{B}}^{(R)}, \\
\mathcal{C} &= \hat{\mathcal{C}} \times_1 \Psi_{\mathbf{A}}^{(1)} \times_2 \Psi_{\mathbf{B}}^{(1)} = \hat{\mathcal{C}} \times_1 \Psi_{\mathbf{A}}^{(2)} \times_2 \Psi_{\mathbf{B}}^{(2)} \\
&\times \cdots \times \hat{\mathcal{C}} \times_1 \Psi_{\mathbf{A}}^{(R)} \times_2 \Psi_{\mathbf{B}}^{(R)},
\end{aligned} \tag{7.48}$$

$$\begin{aligned}
\mathcal{C} &= \hat{\mathcal{C}} \times_1 \Psi_{\mathbf{A}}^{(1)} \times_2 \Psi_{\mathbf{B}}^{(1)} = \hat{\mathcal{C}} \times_1 \Psi_{\mathbf{A}}^{(2)} \times_2 \Psi_{\mathbf{B}}^{(2)} \\
&\times \cdots \times \hat{\mathcal{C}} \times_1 \Psi_{\mathbf{A}}^{(R)} \times_2 \Psi_{\mathbf{B}}^{(R)},
\end{aligned} \tag{7.49}$$

which completes the proof. \square

With Lemma 7.2 in hand, we are now ready to prove Thm. 3.2.

Theorem 3.2. *Suppose the SRI $\mathcal{Z} \in \mathbb{R}^{M_1 \times M_2 \times S}$, HSI $\mathcal{X} \in \mathbb{R}^{m_1 \times m_2 \times S}$, and MSI $\mathcal{Y} \in \mathbb{R}^{M_1 \times M_2 \times S}$ satisfy relationship (2.5). Suppose further that the Tucker decomposition of \mathcal{Z} and the KD of spatial-degradation matrix $\mathbf{D} \in \mathbb{R}^{M_1 M_2 \times m_1 m_2}$ are*

$$\mathcal{Z} = \mathcal{G} \times_1 \mathbf{U}_1 \times_2 \mathbf{U}_2 \times_3 \mathbf{U}_3, \tag{7.50}$$

$$\mathbf{D} = \sum_{r=1}^{\text{kr}_{\mathbf{D}}} (\mathbf{P}_2^{(r)} \otimes \mathbf{P}_1^{(r)})^T, \tag{7.51}$$

where $\mathcal{G} \in \mathbb{R}^{L_1 \times L_2 \times C}$ is drawn from an absolutely continuous distribution; and \mathbf{U}_1 , \mathbf{U}_2 , and \mathbf{U}_3 have full column rank. Then, if it is true that

$$\begin{aligned}
L_1 &\leq L_2 C, \quad L_2 \leq L_1 C, \quad S \geq 3 \\
\text{rank} \left\{ \left[\mathbf{P}_1^{(1)} \mathbf{U}_1, \dots, \mathbf{P}_1^{(\text{kr}_{\mathbf{D}})} \mathbf{U}_1 \right] \right\} &= L_1 \text{kr}_{\mathbf{D}}, \\
\text{rank} \left\{ \left[\mathbf{P}_2^{(1)} \mathbf{U}_2, \dots, \mathbf{P}_2^{(\text{kr}_{\mathbf{D}})} \mathbf{U}_2 \right] \right\} &= L_2 \text{kr}_{\mathbf{D}}, \\
\text{rank} \{ \mathbf{Y}_{[1]} \} &= L_1, \\
\text{rank} \{ \mathbf{Y}_{[2]} \} &= L_2,
\end{aligned} \tag{7.52}$$

any solution of Tucker-rank at most (L_1, L_2, S) to GTF-HSR recovers SRI \mathcal{Z} with probability 1.

Proof. Combining (3.6) with the Tucker decomposition of \mathcal{Z} , we have

$$\mathcal{X} = \sum_{r=1}^{\text{kr}_{\mathbf{D}}} \mathcal{G} \times_1 \mathbf{P}_1^{(r)} \mathbf{U}_1 \times_2 \mathbf{P}_2^{(r)} \mathbf{U}_2 \times_3 \mathbf{U}_3, \tag{7.53}$$

$$\mathcal{Y} = \mathcal{G} \times_1 \mathbf{U}_1 \times_2 \mathbf{U}_2 \times_3 \mathbf{R} \mathbf{U}_3. \tag{7.54}$$

Denoting that

$$\mathbf{P}_1 \triangleq \left[\mathbf{P}_1^{(1)} \mathbf{U}_1, \mathbf{P}_1^{(2)} \mathbf{U}_1, \dots, \mathbf{P}_1^{(R)} \mathbf{U}_1 \right], \tag{7.55}$$

$$\mathbf{P}_2 \triangleq \left[\mathbf{P}_2^{(1)} \mathbf{U}_2, \mathbf{P}_2^{(2)} \mathbf{U}_2, \dots, \mathbf{P}_2^{(R)} \mathbf{U}_2 \right], \tag{7.56}$$

then \mathbf{P}_1 and \mathbf{P}_2 are of full column rank according to our conditions. Considering that \mathbf{U}_3 has full column rank along with the conditions $L_1 \leq L_2 C$, $L_2 \leq L_1 C$, and $S \geq 3$, we are now capable of invoking Lemma 7.2 above and Thm 5.1 in [43] to conclude the essential uniqueness of the decomposition on \mathcal{X} in the form of (7.53) with respect to \mathcal{G} , $\left\{ \mathbf{P}_1^{(r)} \mathbf{U}_1 \right\}_{r=1}^{\text{kr}_{\mathbf{D}}}$, $\left\{ \mathbf{P}_2^{(r)} \mathbf{U}_2 \right\}_{r=1}^{\text{kr}_{\mathbf{D}}}$, and \mathbf{U}_3 .

Now, let $\hat{\mathcal{Z}} \in \mathbb{R}^{M_1 \times M_2 \times S}$ be an arbitrary solution of Tucker-rank at most (L_1, L_2, C) to the GTF-HSR problem of Def. 3.2. Its Tucker decomposition then expands as

$$\hat{\mathcal{Z}} = \hat{\mathcal{G}} \times_1 \hat{\mathbf{U}}_1 \times_2 \hat{\mathbf{U}}_2 \times_3 \hat{\mathbf{U}}_3, \tag{7.57}$$

where $\mathcal{G} \in \mathbb{R}^{\hat{L}_1 \times \hat{L}_2 \times \hat{C}}$ is of Tucker-rank $(\hat{L}_1, \hat{L}_2, \hat{C})$, and $\hat{\mathbf{U}}_1 \in \mathbb{R}^{M_1 \times \hat{L}_1}$, $\hat{\mathbf{U}}_2 \in \mathbb{R}^{M_2 \times \hat{L}_2}$, and $\hat{\mathbf{U}}_3 \in \mathbb{R}^{S \times \hat{C}}$ all have full column rank. Substituting (7.57) into (3.6), we have

$$\mathcal{X} = \sum_{r=1}^{\text{kr}_{\mathbf{D}}} \hat{\mathcal{G}} \times_1 \mathbf{P}_1^{(r)} \hat{\mathbf{U}}_1 \times_2 \mathbf{P}_2^{(r)} \hat{\mathbf{U}}_2 \times_3 \hat{\mathbf{U}}_3, \tag{7.58}$$

$$\mathcal{Y} = \hat{\mathcal{G}} \times_1 \hat{\mathbf{U}}_1 \times_2 \hat{\mathbf{U}}_2 \times_3 \mathbf{R} \hat{\mathbf{U}}_3. \tag{7.59}$$

Then we notice that, from (7.58), we can have only that $\hat{L}_1 = L_1$, $\hat{L}_2 = L_2$, and $\hat{C} = C$ which would otherwise contradict the uniqueness of (7.53) in terms of \mathcal{G} , $\left\{ \mathbf{P}_1^{(r)} \mathbf{U}_1 \right\}_{r=1}^{\text{kr}_{\mathbf{D}}}$, $\left\{ \mathbf{P}_2^{(r)} \mathbf{U}_2 \right\}_{r=1}^{\text{kr}_{\mathbf{D}}}$, and \mathbf{U}_3 . It then follows from such uniqueness that, $\forall r \in \{1, 2, \dots, \text{kr}_{\mathbf{D}}\}$, there exist $\Psi_1^{(r)} \in \mathbb{R}^{L_1 \times L_1}$ and $\Psi_2^{(r)} \in \mathbb{R}^{L_2 \times L_2}$ that are nonsingular matrices such that

$$\mathbf{P}_1^{(r)} \hat{\mathbf{U}}_1 = \mathbf{P}_1^{(r)} \mathbf{U}_1 \Psi_1^{(r)}, \tag{7.60}$$

$$\mathbf{P}_2^{(r)} \hat{\mathbf{U}}_2 = \mathbf{P}_2^{(r)} \mathbf{U}_2 \Psi_2^{(r)}, \tag{7.61}$$

$$\hat{\mathbf{U}}_3 = \mathbf{U}_3 \Psi_3 \tag{7.62}$$

$$\hat{\mathcal{G}} = \mathcal{G} \times_1 \left(\Psi_1^{(r)} \right)^{-1} \times_2 \left(\Psi_2^{(r)} \right)^{-1} \times_3 \left(\Psi_3 \right)^{-1}, \tag{7.63}$$

where $\Psi_3 \in \mathbb{R}^{C \times C}$ is also nonsingular. Subsequently, unfolding (7.54) and (7.59), we have

$$\mathbf{Y}_{[1]} = \mathbf{U}_1 \mathbf{G}_{[1]} \left(\mathbf{P}_3^{(r)} \mathbf{U}_3 \otimes \mathbf{U}_2 \right)^T, \tag{7.64}$$

$$\mathbf{Y}_{[2]} = \mathbf{U}_2 \mathbf{G}_{[2]} \left(\mathbf{P}_3^{(r)} \mathbf{U}_3 \otimes \mathbf{U}_1 \right)^T, \tag{7.65}$$

$$\mathbf{Y}_{[1]} = \hat{\mathbf{U}}_1 \hat{\mathbf{G}}_{[1]} \left(\mathbf{P}_3^{(r)} \hat{\mathbf{U}}_3 \otimes \hat{\mathbf{U}}_2 \right)^T, \tag{7.66}$$

$$\mathbf{Y}_{[2]} = \hat{\mathbf{U}}_2 \hat{\mathbf{G}}_{[2]} \left(\mathbf{P}_3^{(r)} \hat{\mathbf{U}}_3 \otimes \hat{\mathbf{U}}_1 \right)^T. \tag{7.67}$$

Since $\text{rank} \{ \mathbf{Y}_{[1]} \} = L_1$ and $\text{rank} \{ \mathbf{Y}_{[2]} \} = L_2$, it is concluded that

$$\text{col} \left(\mathbf{Y}_{[1]} \right) = \text{col} \left(\mathbf{U}_1 \right) = \text{col} \left(\hat{\mathbf{U}}_1 \right), \tag{7.68}$$

$$\text{col} \left(\mathbf{Y}_{[2]} \right) = \text{col} \left(\mathbf{U}_2 \right) = \text{col} \left(\hat{\mathbf{U}}_2 \right), \tag{7.69}$$

which indicates the existence of nonsingular $\mathbf{Q}_1 \in \mathbb{R}^{L_1 \times L_1}$ and $\mathbf{Q}_2 \in \mathbb{R}^{L_2 \times L_2}$ such that

$$\hat{\mathbf{U}}_1 = \mathbf{U}_1 \mathbf{Q}_1, \tag{7.70}$$

$$\hat{\mathbf{U}}_2 = \mathbf{U}_2 \mathbf{Q}_2. \tag{7.71}$$

We then have that

$$\mathbf{P}_1^{(r)} \hat{\mathbf{U}}_1 = \mathbf{P}_1^{(r)} \mathbf{U}_1 \mathbf{Q}_1 = \mathbf{P}_1^{(r)} \mathbf{U}_1 \Psi_1^{(r)}, \tag{7.72}$$

$$\mathbf{P}_2^{(r)} \hat{\mathbf{U}}_2 = \mathbf{P}_2^{(r)} \mathbf{U}_2 \mathbf{Q}_2 = \mathbf{P}_2^{(r)} \mathbf{U}_2 \Psi_2^{(r)}. \tag{7.73}$$

Since $\mathbf{P}_1^{(r)} \mathbf{U}_1$ has full column rank, it is then true that, $\forall r \in \{1, 2, \dots, \text{kr}_{\mathbf{D}}\}$,

$$\mathbf{Q}_1 = \Psi_1^{(r)}, \tag{7.74}$$

$$\mathbf{Q}_2 = \Psi_2^{(r)}. \tag{7.75}$$

It finally follows that

$$\begin{aligned}
\hat{\mathcal{Z}} &= \hat{\mathcal{G}} \times_1 \hat{\mathbf{U}}_1 \times_2 \hat{\mathbf{U}}_2 \times_3 \hat{\mathbf{U}}_3 \\
&= \hat{\mathcal{G}} \times_1 \mathbf{U}_1 \mathbf{Q}_1 \times_2 \mathbf{U}_2 \mathbf{Q}_2 \times_3 \mathbf{U}_3 \Psi_3
\end{aligned}$$

$$\begin{aligned}
&= \mathcal{G} \times_1 \left(\Psi_1^{(r)} \right)^{-1} \times_2 \left(\Psi_2^{(r)} \right)^{-1} \times_3 \left(\Psi_3 \right)^{-1} \\
&\quad \times_1 \mathbf{U}_1 \mathbf{Q}_1 \times_2 \mathbf{U}_2 \mathbf{Q}_2 \times_3 \mathbf{U}_3 \Psi_3 \\
&= \mathcal{G} \times_1 \left(\mathbf{Q}_1 \right)^{-1} \times_2 \left(\mathbf{Q}_2 \right)^{-1} \times_3 \left(\Psi_3 \right)^{-1} \\
&\quad \times_1 \mathbf{U}_1 \mathbf{Q}_1 \times_2 \mathbf{U}_2 \mathbf{Q}_2 \times_3 \mathbf{U}_3 \Psi_3 \\
&= \mathcal{G} \times_1 \mathbf{U}_1 \mathbf{Q}_1 \left(\mathbf{Q}_1 \right)^{-1} \times_2 \mathbf{U}_2 \mathbf{Q}_2 \left(\mathbf{Q}_2 \right)^{-1} \times_3 \mathbf{U}_3 \Psi_3 \left(\Psi_3 \right)^{-1} \\
&= \mathcal{G} \times_1 \mathbf{U}_1 \times_2 \mathbf{U}_2 \times_3 \mathbf{U}_3 \\
&= \mathcal{Z}, \tag{7.76}
\end{aligned}$$

which completes the proof. \square

7.4 Proof of Cor. 3.1

Corollary 3.1. *Under the conditions of Thm. 3.2, if it is true that*

$$\begin{aligned}
L_1 &\leq L_2 C, \quad L_2 \leq L_1 C, \quad S \geq 3, \\
\text{rank} \left\{ \left[\mathbf{P}_1^{(1)} \mathbf{U}_1, \dots, \mathbf{P}_1^{(\text{kr}_D)} \mathbf{U}_1 \right] \right\} &= L_1 \text{kr}_D, \tag{7.77} \\
\text{rank} \left\{ \left[\mathbf{P}_2^{(1)} \mathbf{U}_2, \dots, \mathbf{P}_2^{(\text{kr}_D)} \mathbf{U}_2 \right] \right\} &= L_2 \text{kr}_D,
\end{aligned}$$

then any solution to TF-HSR recovers SRI \mathcal{Z} with probability 0 when $\text{kr}_D > 1$.

Proof. We first recall that, under these conditions, we have the essential uniqueness of the decomposition of the HSI \mathcal{X} in the form of

$$\mathcal{X} = \sum_{r=1}^{\text{kr}_D} \mathcal{G} \times_1 \mathbf{P}_1^{(r)} \mathbf{U}_1 \times_2 \mathbf{P}_2^{(r)} \mathbf{U}_2 \times_3 \mathbf{U}_3 \tag{7.78}$$

almost surely. Thus, if SRI \mathcal{Z} solves TF-HSR, there would exist an alternative decomposition of \mathcal{X} in the form of

$$\mathcal{X} = \mathcal{G} \times_1 \mathbf{P}_1 \mathbf{U}_1 \times_2 \mathbf{P}_2 \mathbf{U}_2 \times_3 \mathbf{U}_3, \tag{7.79}$$

which would contradict the uniqueness above. As such, we assert that SRI \mathcal{Z} solves the TF-HSR problem with probability 0, thereby completing the proof. \square

8 DETAILED ADMM DERIVATIONS FOR ALGS. 1 AND 2

8.1 ADMM for Alg. 1

ADMM is used in Alg. 1 to solve the optimization in (4.10), namely,

$$\begin{aligned}
\min_{\mathbf{U}_i^{\mathcal{X}}, \mathbf{A}_i} & \left\| \mathbf{X}_{[i]} - \left[\mathbf{P}_i^{(1)} \quad \dots \quad \mathbf{P}_i^{(\text{kr}_D)} \right] \left(\mathbf{I}_{\text{kr}_D} \otimes \left[\mathbf{U}_i^{\mathcal{Y}} \quad \mathbf{U}_i^{\mathcal{X}} \right] \right) \mathbf{B}_i \right\|_F^2 \\
& + \mu \|\mathbf{A}_i\|_1 \\
\text{s.t.} & \quad \mathbf{A}_i = \mathbf{B}_i,
\end{aligned} \tag{8.1}$$

The augmented Lagrangian function is

$$\begin{aligned}
\mathbf{L} \left(\mathbf{U}_i^{\mathcal{X}}, \mathbf{B}_i, \mathbf{A}_i, \mathbf{M}_i \right) \\
&\triangleq \left\| \mathbf{X}_{[i]} - \left[\mathbf{P}_i^{(1)}, \dots, \mathbf{P}_i^{(\text{kr}_D)} \right] \left(\mathbf{I}_{\text{kr}_D} \otimes \left[\mathbf{U}_i^{\mathcal{Y}}, \mathbf{U}_i^{\mathcal{X}} \right] \right) \mathbf{B}_i \right\|_F^2 \\
&+ \mu \|\mathbf{A}_i\|_1 + \langle \mathbf{M}_i, \mathbf{A}_i - \mathbf{B}_i \rangle + \frac{\rho}{2} \|\mathbf{A}_i - \mathbf{B}_i\|_F^2 \\
&= \left\| \mathbf{X}_{[i]} - \left[\mathbf{P}_i^{(1)}, \dots, \mathbf{P}_i^{(\text{kr}_D)} \right] \left(\mathbf{I}_{\text{kr}_D} \otimes \left[\mathbf{U}_i^{\mathcal{Y}}, \mathbf{U}_i^{\mathcal{X}} \right] \right) \mathbf{B}_i \right\|_F^2 \\
&+ \mu \|\mathbf{A}_i\|_1 + \frac{\rho}{2} \left\| \mathbf{A}_i - \mathbf{B}_i + \frac{\mathbf{M}_i}{\rho} \right\|_F^2 - \frac{\|\mathbf{M}_i\|_F^2}{2\rho},
\end{aligned} \tag{8.2}$$

where the auxiliary variables \mathbf{M}_i are of the same size as \mathbf{A}_i .

- The $\mathbf{U}_i^{\mathcal{X}}$ subproblem:
Solving for $\mathbf{U}_i^{\mathcal{X}}$ proceeds by solving

$$\begin{aligned}
\min_{\mathbf{U}_i^{\mathcal{X}}} \mathbf{L}_{\mathbf{U}_i^{\mathcal{X}}} &\triangleq \left\| \mathbf{X}_{[i]} - \left[\mathbf{P}_i^{(1)} \quad \dots \quad \mathbf{P}_i^{(\text{kr}_D)} \right] \right. \\
&\quad \left. \times \left(\mathbf{I}_{\text{kr}_D} \otimes \left[\mathbf{U}_i^{\mathcal{Y}} \quad \mathbf{U}_i^{\mathcal{X}} \right] \right) \mathbf{B}_i \right\|_F^2.
\end{aligned} \tag{8.3}$$

Partitioning \mathbf{B}_i into

$$\begin{aligned}
\mathbf{B}_i &= \left[\left(\mathbf{B}_i^{(1)\mathcal{Y}} \right)^T, \left(\mathbf{B}_i^{(1)\mathcal{X}} \right)^T, \left(\mathbf{B}_i^{(2)\mathcal{Y}} \right)^T, \left(\mathbf{B}_i^{(2)\mathcal{X}} \right)^T, \right. \\
&\quad \left. \dots \left(\mathbf{B}_i^{(\text{kr}_D)\mathcal{Y}} \right)^T, \left(\mathbf{B}_i^{(\text{kr}_D)\mathcal{X}} \right)^T \right]^T
\end{aligned} \tag{8.4}$$

where $\mathbf{B}_i^{(r)\mathcal{Y}} \in \mathbb{R}^{K_i \times m_{3-i} S}$ and $\mathbf{B}_i^{(r)\mathcal{X}} \in \mathbb{R}^{(L_i - K_i) \times m_{3-i} S}$, $\mathbf{L}_{\mathbf{U}_i^{\mathcal{X}}}$ is then reorganized as

$$\begin{aligned}
\mathbf{L}_{\mathbf{U}_i^{\mathcal{X}}} &= \left\| \mathbf{X}_{[i]} - \left[\mathbf{P}_i^{(1)} \quad \dots \quad \mathbf{P}_i^{(\text{kr}_D)} \right] \right. \\
&\quad \left. \times \left(\mathbf{I}_{\text{kr}_D} \otimes \left[\mathbf{U}_i^{\mathcal{Y}} \quad \mathbf{U}_i^{\mathcal{X}} \right] \right) \mathbf{B}_i \right\|_F^2 \\
&= \left\| \mathbf{X}_{[i]} - \sum_{r=1}^{\text{kr}_D} \mathbf{P}_i^{(r)} \left[\mathbf{U}_i^{\mathcal{Y}} \quad \mathbf{U}_i^{\mathcal{X}} \right] \begin{bmatrix} \mathbf{B}_i^{(r)\mathcal{Y}} \\ \mathbf{B}_i^{(r)\mathcal{X}} \end{bmatrix} \right\|_F^2 \\
&= \left\| \mathbf{X}_{[i]} - \sum_{r=1}^{\text{kr}_D} \mathbf{P}_i^{(r)} \mathbf{U}_i^{\mathcal{Y}} \mathbf{B}_i^{(r)\mathcal{Y}} \right. \\
&\quad \left. - \sum_{r=1}^{\text{kr}_D} \mathbf{P}_i^{(r)} \mathbf{U}_i^{\mathcal{X}} \mathbf{B}_i^{(r)\mathcal{X}} \right\|_F^2.
\end{aligned} \tag{8.5}$$

Thus, the gradient $\nabla \mathbf{L}_{\mathbf{U}_i^{\mathcal{X}}}$ is becomes

$$\begin{aligned}
\nabla \mathbf{L}_{\mathbf{U}_i^{\mathcal{X}}} &= 2 \left(\sum_{r_1=1}^{\text{kr}_D} \sum_{r_2=1}^{\text{kr}_D} \left(\mathbf{P}_i^{r_1} \right)^T \mathbf{P}_i^{r_2} \mathbf{U}_i^{\mathcal{X}} \mathbf{B}_i^{(r_2)\mathcal{X}} \right. \\
&\quad \left. \times \left(\mathbf{B}_i^{(r_1)\mathcal{X}} \right)^T - \sum_{r=1}^{\text{kr}_D} \left(\mathbf{P}_i^r \right)^T \tilde{\mathbf{X}}_{[i]} \left(\mathbf{B}_i^{(r)\mathcal{X}} \right)^T \right),
\end{aligned} \tag{8.6}$$

where $\tilde{\mathbf{X}}_{[i]} \triangleq \mathbf{X}_{[i]} - \sum_{r=1}^{\text{kr}_D} \mathbf{P}_i^{(r)} \mathbf{U}_i^{\mathcal{Y}} \mathbf{B}_i^{(r)\mathcal{Y}}$. Then (8.3) is solved by setting $\nabla \mathbf{L}_{\mathbf{U}_i^{\mathcal{X}}} = 0$ and applying CG [45].

- The \mathbf{B}_i subproblem:
Solving for \mathbf{B}_i proceeds by solving

$$\begin{aligned}
\min_{\mathbf{B}_i} & \left\| \mathbf{X}_{[i]} - \left[\mathbf{P}_i^{(1)} \quad \dots \quad \mathbf{P}_i^{(\text{kr}_D)} \right] \left(\mathbf{I}_{\text{kr}_D} \otimes \left[\mathbf{U}_i^{\mathcal{Y}} \quad \mathbf{U}_i^{\mathcal{X}} \right] \right) \right. \\
&\quad \left. \times \mathbf{B}_i \right\|_F^2 + \frac{\rho}{2} \left\| \mathbf{A}_i - \mathbf{B}_i + \frac{\mathbf{M}_i}{\rho} \right\|_F^2.
\end{aligned} \tag{8.7}$$

The corresponding objective function is strongly convex and has the unique solution

$$\begin{aligned}
\mathbf{B}_i &= \left(\mathbf{D}_i^T \mathbf{D}_i + \frac{\rho}{2} \mathbf{I}_{L_i \text{kr}_D} \right)^{-1} \\
&\quad \times \left(\mathbf{D}_i^T \mathbf{X}_{[i]} + \frac{\rho}{2} \left(\mathbf{A}_i + \frac{\mathbf{M}_i}{\rho} \right) \right),
\end{aligned} \tag{8.8}$$

where

$$\mathbf{D}_i \triangleq \left[\mathbf{P}_i^{(1)} \quad \dots \quad \mathbf{P}_i^{(\text{kr}_D)} \right] \left(\mathbf{I}_{\text{kr}_D} \otimes \left[\mathbf{U}_i^{\mathcal{Y}} \quad \mathbf{U}_i^{\mathcal{X}} \right] \right).$$

- The \mathbf{A}_i subproblem:
The solution to

$$\min_{\mathbf{A}_i} \mu \|\mathbf{A}_i\|_1 + \frac{\rho}{2} \left\| \mathbf{A}_i - \mathbf{B}_i + \frac{\mathbf{M}_i}{\rho} \right\|_F^2 \quad (8.9)$$

is well-known to be

$$\mathbf{A}_i = \text{soft} \left(\mathbf{B}_i - \frac{\mathbf{M}_i}{\rho}, \frac{\mu}{\rho} \right). \quad (8.10)$$

- Updating \mathbf{M}_i :
The final step is the updating of the auxiliary variables \mathbf{M}_i which is done as

$$\mathbf{M}_i \leftarrow \mathbf{M}_i + \rho(\mathbf{A}_i - \mathbf{B}_i). \quad (8.11)$$

8.2 ADMM for Alg. 2

ADMM is used in Alg. 2 to solve the optimization in (4.13), namely

$$\begin{aligned} & \min_{\{\mathcal{G}_r\}_{r=1}^{\text{krD}}, \mathcal{G}, \hat{\mathbf{G}}} \|\hat{\mathbf{G}}\|_{2,\gamma} \\ \text{s.t. } & \mathcal{X} = \sum_{r=1}^{\text{krD}} \mathcal{G}_r \times_1 \mathbf{P}_1^{(r)} \mathbf{U}_1 \times_2 \mathbf{P}_2^{(r)} \mathbf{U}_2 \times_3 \mathbf{U}_3, \\ & \mathcal{Y} = \mathcal{G} \times_1 \mathbf{U}_1 \times_2 \mathbf{U}_2 \times_3 \mathbf{R} \mathbf{U}_3, \\ & \hat{\mathbf{G}} = \mathbf{G}_{[t]}, \\ & \mathcal{G} = \mathcal{G}_r, \quad r = 1, 2, \dots, \text{krD}. \end{aligned} \quad (8.12)$$

The augmented Lagrangian function is

$$\begin{aligned} & \mathcal{L}(\{\mathcal{G}_r\}_{r=1}^{\text{krD}}, \mathcal{G}, \hat{\mathbf{G}}, \mathcal{P}^{\mathcal{X}}, \mathcal{P}^{\mathcal{Y}}, \mathbf{W}, \{\mathcal{P}_r\}_{r=1}^{\text{krD}}) \\ & \triangleq \|\hat{\mathbf{G}}\|_{2,\gamma} + \left\langle \mathcal{P}^{\mathcal{X}}, \mathcal{X} - \sum_{r=1}^{\text{krD}} \mathcal{G}_r \times_1 \mathbf{P}_1^{(r)} \mathbf{U}_1 \times_2 \mathbf{P}_2^{(r)} \mathbf{U}_2 \times_3 \mathbf{U}_3 \right\rangle \\ & + \left\langle \mathcal{P}^{\mathcal{Y}}, \mathcal{Y} - \mathcal{G} \times_1 \mathbf{U}_1 \times_2 \mathbf{U}_2 \times_3 \mathbf{R} \mathbf{U}_3 \right\rangle + \left\langle \mathbf{W}, \hat{\mathbf{G}} - \mathbf{G}_{[B;t]} \right\rangle \\ & + \sum_{r=1}^{\text{krD}} \langle \mathcal{P}_r, \mathcal{G} - \mathcal{G}_r \rangle \\ & + \frac{\rho}{2} \left(\left\| \mathcal{X} - \sum_{r=1}^{\text{krD}} \mathcal{G}_r \times_1 \mathbf{P}_1^{(r)} \mathbf{U}_1 \times_2 \mathbf{P}_2^{(r)} \mathbf{U}_2 \times_3 \mathbf{U}_3 \right\|_F^2 \right. \\ & \quad \left. + \|\mathcal{Y} - \mathcal{G} \times_1 \mathbf{U}_1 \times_2 \mathbf{U}_2 \times_3 \mathbf{R} \mathbf{U}_3\|_F^2 \right. \\ & \quad \left. + \|\hat{\mathbf{G}} - \mathbf{G}_{[B;t]}\|_F^2 + \sum_{r=1}^{\text{krD}} \|\mathcal{G} - \mathcal{G}_r\|_F^2 \right) = \|\hat{\mathbf{G}}\|_{2,\gamma} \\ & + \frac{\rho}{2} \left(\left\| \mathcal{X} - \sum_{r=1}^{\text{krD}} \mathcal{G}_r \times_1 \mathbf{P}_1^{(r)} \mathbf{U}_1 \times_2 \mathbf{P}_2^{(r)} \mathbf{U}_2 \times_3 \mathbf{U}_3 + \frac{\mathcal{P}^{\mathcal{X}}}{\rho} \right\|_F^2 \right. \\ & \quad \left. + \left\| \mathcal{Y} - \mathcal{G} \times_1 \mathbf{U}_1 \times_2 \mathbf{U}_2 \times_3 \mathbf{R} \mathbf{U}_3 + \frac{\mathcal{P}^{\mathcal{Y}}}{\rho} \right\|_F^2 \right. \\ & \quad \left. + \left\| \hat{\mathbf{G}} - \mathbf{G}_{[B;t]} + \frac{\mathbf{W}}{\rho} \right\|_F^2 + \sum_{r=1}^{\text{krD}} \left\| \mathcal{G} - \mathcal{G}_r + \frac{\mathcal{P}_r}{\rho} \right\|_F^2 \right) \\ & - \frac{1}{2\rho} \left(\|\mathcal{P}^{\mathcal{X}}\|_F^2 + \|\mathcal{P}^{\mathcal{Y}}\|_F^2 + \|\mathbf{W}\|_F^2 + \sum_{r=1}^{\text{krD}} \|\mathcal{P}_r\|_F^2 \right) \end{aligned} \quad (8.13)$$

where $\mathcal{P}^{\mathcal{X}}$, $\mathcal{P}^{\mathcal{Y}}$, \mathbf{W} , and $\{\mathcal{P}_r\}_{r=1}^{\text{krD}}$ are auxiliary variables.

- The \mathcal{G}_r subproblem:
Solving for \mathcal{G}_r proceeds by solving

$$\begin{aligned} \min_{\mathcal{G}_r} \mathcal{L}_{\mathcal{G}_r} & \triangleq \left\| \mathcal{X} - \sum_{r^*=1}^{\text{krD}} \mathcal{G}_{r^*} \times_1 \mathbf{P}_1^{(r^*)} \mathbf{U}_1 \times_2 \mathbf{P}_2^{(r^*)} \mathbf{U}_2 \right. \\ & \quad \left. \times_3 \mathbf{U}_3 + \frac{\mathcal{P}^{\mathcal{X}}}{\rho} \right\|_F^2 + \left\| \mathcal{G} - \mathcal{G}_r + \frac{\mathcal{P}_r}{\rho} \right\|_F^2 \\ & = \left\| \mathcal{X} + \frac{\mathcal{P}^{\mathcal{X}}}{\rho} - \sum_{r^* \neq r} \mathcal{G}_{r^*} \times_1 \mathbf{P}_1^{(r^*)} \mathbf{U}_1 \right. \\ & \quad \left. \times_2 \mathbf{P}_2^{(r^*)} \mathbf{U}_2 \times_3 \mathbf{U}_3 - \mathcal{G}_r \times_1 \mathbf{P}_1^{(r)} \mathbf{U}_1 \right. \\ & \quad \left. \times_2 \mathbf{P}_2^{(r)} \mathbf{U}_2 \times_3 \mathbf{U}_3 \right\|_F^2 \\ & \quad + \left\| \mathcal{G}_r - \left(\mathcal{G} + \frac{\mathcal{P}_r}{\rho} \right) \right\|_F^2. \end{aligned} \quad (8.14)$$

By defining

$$\begin{aligned} \mathcal{H} & = \mathcal{X} + \frac{\mathcal{P}^{\mathcal{X}}}{\rho} \\ & - \sum_{r^* \neq r} \mathcal{G}_{r^*} \times_1 \mathbf{P}_1^{(r^*)} \mathbf{U}_1 \times_2 \mathbf{P}_2^{(r^*)} \mathbf{U}_2 \times_3 \mathbf{U}_3, \end{aligned} \quad (8.15)$$

$$\mathbf{Q}_1 = \mathbf{P}_1^{(r)} \mathbf{U}_1, \quad (8.16)$$

$$\mathbf{Q}_2 = \mathbf{P}_2^{(r)} \mathbf{U}_2, \quad (8.17)$$

$$\mathbf{Q}_3 = \mathbf{U}_3, \quad (8.18)$$

$$\mathcal{S} = \mathcal{G}_r, \quad (8.19)$$

$$\mathcal{K} = \mathcal{G} + \frac{\mathcal{P}_r}{\rho}, \quad (8.20)$$

(8.14) then falls into the form

$$\min_{\mathcal{S}} \|\mathcal{H} - \mathcal{S} \times_1 \mathbf{Q}_1 \times_2 \mathbf{Q}_2 \times_3 \mathbf{Q}_3\|_F^2 + \tau \|\mathcal{S} - \mathcal{K}\|_F^2, \quad (8.21)$$

where $\tau = 1$. To optimize (8.21), we first denote the eigenvalue decompositions of $\mathbf{Q}_1^T \mathbf{Q}_1$, $\mathbf{Q}_2^T \mathbf{Q}_2$, and $\mathbf{Q}_3^T \mathbf{Q}_3$ as

$$\mathbf{Q}_1^T \mathbf{Q}_1 = \mathbf{V}_1 \boldsymbol{\Sigma}_1 \mathbf{V}_1^T \quad (8.22)$$

$$\mathbf{Q}_2^T \mathbf{Q}_2 = \mathbf{V}_2 \boldsymbol{\Sigma}_2 \mathbf{V}_2^T \quad (8.23)$$

$$\mathbf{Q}_3^T \mathbf{Q}_3 = \mathbf{V}_3 \boldsymbol{\Sigma}_3 \mathbf{V}_3^T, \quad (8.24)$$

respectively. Then, letting $\mathcal{T} = \mathcal{H} \times_1 \mathbf{Q}_1^T \times_2 \mathbf{Q}_2^T \times_3 \mathbf{Q}_3^T + \tau \mathcal{K}$ and $\mathcal{T}' = \mathcal{T} \times_1 \mathbf{V}_1^T \times_2 \mathbf{V}_2^T \times_3 \mathbf{V}_3^T$, the optimal solution is obtained via

$$\mathcal{S} = \mathcal{T}'' \times_1 \mathbf{V}_1 \times_2 \mathbf{V}_2 \times_3 \mathbf{V}_3, \quad (8.25)$$

where

$$\text{Vec}(\mathcal{T}'') = (\boldsymbol{\Sigma}_3 \otimes \boldsymbol{\Sigma}_2 \otimes \boldsymbol{\Sigma}_1 + \tau \mathbf{I}_{L_1 L_2 C})^{-1} \text{Vec}(\mathcal{T}').$$

- The $\hat{\mathbf{G}}$ subproblem:
Solving for $\hat{\mathbf{G}}$ requires solving

$$\min_{\hat{\mathbf{G}}} \frac{\rho}{2} \left\| \hat{\mathbf{G}} - \mathbf{G}_{[B;t]} + \frac{\mathbf{W}}{\rho} \right\|_F^2 + \|\hat{\mathbf{G}}\|_{2,\gamma}, \quad (8.26)$$

which is a nonconvex, sparsity-inducing problem. We resort to the recently developed GAI [48] for an iterative solution.

- The \mathcal{G} subproblem:
To find \mathcal{G} , we solve

$$\min_{\mathcal{G}} \left\| \mathcal{Y} - \mathcal{G} \times_1 \mathbf{U}_1 \times_2 \mathbf{U}_2 \times_3 \mathbf{R}\mathbf{U}_3 + \frac{\mathcal{P}^{\mathcal{Y}}}{\rho} \right\|_F^2 + \left\| \hat{\mathbf{G}} - \mathbf{G}_{[B;t]} + \frac{\mathbf{W}}{\rho} \right\|_F^2 + \sum_{r=1}^{\text{kr}_D} \left\| \mathcal{G} - \mathcal{G}_r + \frac{\mathcal{P}_r}{\rho} \right\|_F^2.$$

Introducing the variables

$$\mathcal{H} = \mathcal{Y} + \frac{\mathcal{P}^{\mathcal{Y}}}{\rho}, \quad (8.27)$$

$$\mathcal{S} = \mathcal{G}, \quad (8.28)$$

$$\mathbf{Q}_1 = \mathbf{U}_1, \quad (8.29)$$

$$\mathbf{Q}_2 = \mathbf{U}_2, \quad (8.30)$$

$$\mathbf{Q}_3 = \mathbf{R}\mathbf{U}_3, \quad (8.31)$$

$$\mathcal{K} = \frac{\left(\mathcal{G}^{\mathbf{W}} + \sum_{r=1}^{\text{kr}_D} \mathcal{G}_r - \frac{\mathcal{P}_r}{\rho} \right)}{\text{kr}_D + 1}, \quad (8.32)$$

$$\tau = \text{kr}_D + 1, \quad (8.33)$$

where $\mathbf{G}_{[t]}^{\mathbf{W}} \triangleq \hat{\mathbf{G}} + \frac{\mathbf{W}}{\rho}$ is the B-unfolding of $\mathcal{G}^{\mathbf{W}}$, problem (8.27) is equivalent to (8.21) and can be optimized similarly.

- Updating $\mathcal{P}^{\mathcal{X}}$, $\mathcal{P}^{\mathcal{Y}}$, \mathbf{W} , $\{\mathcal{P}_r\}_{r=1}^{\text{kr}_D}$:
Updating the auxiliary variables is done as

$$\mathcal{P}^{\mathcal{X}} \leftarrow \mathcal{P}^{\mathcal{X}} + \rho \left(\mathcal{X} - \sum_{r=1}^{\text{kr}_D} \mathcal{G}_r \times_1 \mathbf{P}_1^{(r)} \mathbf{U}_1 \times_2 \mathbf{P}_2^{(r)} \mathbf{U}_2 \times_3 \mathbf{U}_3 \right), \quad (8.34)$$

$$\mathcal{P}^{\mathcal{Y}} \leftarrow \mathcal{P}^{\mathcal{Y}} + \rho (\mathcal{Y} - \mathcal{G} \times_1 \mathbf{U}_1 \times_2 \mathbf{U}_2 \times_3 \mathbf{R}\mathbf{U}_3), \quad (8.35)$$

$$\mathbf{W} \leftarrow \mathbf{W} + \rho (\hat{\mathbf{G}} - \mathbf{G}_{[t]}), \quad (8.36)$$

$$\mathcal{P}_r \leftarrow \mathcal{P}_r + \rho (\mathcal{G} - \mathcal{G}_r), \quad r = 1, 2, \dots, \text{kr}_D. \quad (8.37)$$

REFERENCES

- [1] N. Yokoya, C. Grohnfeldt, and J. Chanussot, "Hyperspectral and multispectral data fusion: A comparative review of the recent literature," *IEEE Geoscience and Remote Sensing Magazine*, vol. 5, no. 2, pp. 29–56, 2017.
- [2] S. Chen, L. Zhang, and L. Zhang, "Msdformer: Multiscale deformable transformer for hyperspectral image super-resolution," *IEEE Transactions on Geoscience and Remote Sensing*, vol. 61, pp. 1–14, 2023.
- [3] R. Molina, A. K. Katsaggelos, and J. Mateos, "Bayesian and regularization methods for hyperparameter estimation in image restoration," vol. 8, no. 2, pp. 231–246, Feb. 1999.
- [4] R. C. Hardie, M. T. Eismann, and G. L. Wilson, "MAP estimation for hyperspectral image resolution enhancement using an auxiliary sensor," vol. 13, no. 9, pp. 1174–1184, Sep. 2004.
- [5] R. Kawakami, Y. Matsushita, J. Wright, M. Ben-Ezra, Y.-W. Tai, and K. Ikeuchi, "High-resolution hyperspectral imaging via matrix factorization," Colorado Springs, CO, Jun. 2011, pp. 2329–2336.
- [6] N. Yokoya, T. Yairi, and A. Iwasaki, "Coupled nonnegative matrix factorization unmixing for hyperspectral and multispectral data fusion," vol. 50, no. 2, pp. 528–537, Feb. 2012.
- [7] C. Lanaras, E. Baltsavias, and K. Schindler, "Hyperspectral super-resolution by coupled spectral unmixing," Santiago, Chile, Dec. 2015, pp. 3586–3594.
- [8] Q. Wei, J. M. Bioucas-Dias, N. Dobigeon, J.-Y. Tourneret, M. Chen, and S. Godsill, "Multiband image fusion based on spectral unmixing," vol. 54, no. 12, pp. 7236–7249, Dec. 2016.
- [9] C.-H. Lin, F. Ma, C.-Y. Chi, and C.-H. Hsieh, "A convex optimization-based coupled nonnegative matrix factorization algorithm for hyperspectral and multispectral data fusion," vol. 56, no. 3, pp. 1652–1667, Mar. 2018.
- [10] N. Akhtar, F. Shafait, and A. Mian, "Sparse spatio-spectral representation for hyperspectral image super-resolution," Zurich, Switzerland, Sep. 2014, pp. 63–78.
- [11] W. Dong, F. Fu, G. Shi, X. Cao, J. Wu, G. Li, and X. Li, "Hyperspectral image super-resolution via non-negative structured sparse representation," vol. 25, no. 5, pp. 2337–2352, May 2016.
- [12] X.-H. Han, B. Shi, and Y. Zheng, "Self-similarity constrained sparse representation for hyperspectral image super-resolution," vol. 27, no. 11, pp. 5625–5637, Nov. 2018.
- [13] M. Simões, J. Bioucas-Dias, L. B. Almeida, and J. Chanussot, "A convex formulation for hyperspectral image super-resolution via subspace-based regularization," vol. 53, no. 6, pp. 3373–3388, Jun. 2015.
- [14] X. Han, J. Yu, J.-H. Xue, and W. Sun, "Hyperspectral and multispectral image fusion using optimized twin dictionaries," vol. 29, pp. 4709–4720.
- [15] J. Xue, Y.-Q. Zhao, Y. Bu, W. Liao, J. C.-W. Chan, and W. Philips, "Spatial-spectral structured sparse low-rank representation for hyperspectral image super-resolution," vol. 30, pp. 3084–3097, 2021.
- [16] R. Dian and S. Li, "Hyperspectral image super-resolution via subspace-based low tensor multi-rank regularization," vol. 28, no. 10, pp. 5135–5146, Oct. 2019.
- [17] N. Liu, L. Li, W. Li, R. Tao, J. E. Fowler, and J. Chanussot, "Hyperspectral restoration and fusion with multispectral imagery by recasting low-rank tensor-approximation," vol. 59, no. 9, pp. 7817–7830, Sep. 2021.
- [18] W. He, Q. Yao, C. Li, N. Yokoya, Q. Zhao, H. Zhang, and L. Zhang, "Non-local meets global: An iterative paradigm for hyperspectral image restoration," vol. 44, no. 4, pp. 2089–2107, Apr. 2022.
- [19] N. Akhtar, F. Shafait, and A. Mian, "Bayesian sparse representation for hyperspectral image super resolution," Boston, MA, Jun. 2015, pp. 3631–3640.
- [20] Q. Wei, N. Dobigeon, and J.-Y. Tourneret, "Fast fusion of multi-band images based on solving a Sylvester equation," vol. 24, no. 11, pp. 4109–4121, Nov. 2015.
- [21] Z. Wang, B. Chen, H. Zhang, and H. Liu, "Unsupervised hyperspectral and multispectral images fusion based on nonlinear variational probabilistic generative model," vol. 33, no. 2, pp. 721–735, Feb. 2022.
- [22] W. Dong, J. Qu, S. Xiao, T. Zhang, Y. Li, and X. Jia, "Noise prior knowledge informed Bayesian inference network for hyperspectral super-resolution," vol. 32, pp. 3121–3135.
- [23] H. V. Nguyen, M. O. Ulfarsson, J. R. Sveinsson, and M. Dalla Mura, "Deep SURE for unsupervised remote sensing image fusion," vol. 60, 2022.
- [24] R. Dian, A. Guo, and S. Li, "Zero-shot hyperspectral sharpening," vol. 45, no. 10, pp. 12 650–12 666, Oct. 2023.
- [25] Q. Xie, M. Zhou, Q. Zhao, Z. Xu, and D. Meng, "MHF-Net: An interpretable deep network for multispectral and hyperspectral image fusion," vol. 44, no. 3, pp. 1457–1473, Mar. 2022.
- [26] R. Dian, L. Fang, and S. Li, "Hyperspectral image super-resolution via non-local sparse tensor factorization," Honolulu, HI, Jul. 2017, pp. 3862–3871.
- [27] Y. Chen, T.-Z. Huang, W. He, N. Yokoya, and X.-L. Zhao, "Hyperspectral image compressive sensing reconstruction using subspace-based nonlocal tensor ring decomposition," vol. 29, pp. 6813–6828, 2020.
- [28] C. I. Kanatsoulis, X. Fu, N. D. Sidiropoulos, and W.-K. Ma, "Hyperspectral super-resolution: A coupled tensor factorization approach," vol. 66, no. 24, pp. 6503–6517, Dec. 2018.
- [29] S. Li, R. Dian, L. Fang, and J. M. Bioucas-Dias, "Fusing hyperspectral and multispectral images via coupled sparse tensor factorization," vol. 27, no. 8, pp. 4118–4130, Aug. 2018.
- [30] C. Prévost, K. Usevich, P. Comon, and D. Brie, "Hyperspectral super-resolution with coupled Tucker approximation: Recoverability and SVD-based algorithms," vol. 68, pp. 931–946, 2020.
- [31] M. Ding, X. Fu, T.-Z. Huang, J. Wang, and X.-L. Zhao, "Hyperspectral super-resolution via interpretable block-term tensor modeling," vol. 15, no. 4, pp. 641–656, Apr. 2021.
- [32] Y. Bu, Y. Zhao, J. Xue, J. C.-W. Chan, S. G. Kong, C. Yi, J. Wen, and B. Wang, "Hyperspectral and multispectral image fusion via

- graph Laplacian-guided coupled tensor decomposition," vol. 21, no. 1, pp. 648–662, Jan. 2021.
- [33] W. Wan, W. Guo, H. Huang, and J. Liu, "Nonnegative and non-local sparse tensor factorization-based hyperspectral image super-resolution," vol. 58, no. 12, pp. 8384–8394, Dec. 2020.
- [34] Y. Xu, Z. Wu, J. Chanussot, and Z. Wei, "Hyperspectral images super-resolution via learning high-order coupled tensor ring representation," *IEEE Transactions on Neural Networks and Learning Systems*, vol. 31, no. 11, pp. 4747–4760, Nov. 2020.
- [35] J. Yang, L. Xiao, Y.-Q. Zhao, and J. C.-W. Chan, "Unsupervised deep tensor network for hyperspectral-multispectral image fusion," to appear.
- [36] Y. Xu, Z. Wu, J. Chanussot, P. Comon, and Z. Wei, "Nonlocal coupled tensor CP decomposition for hyperspectral and multispectral image fusion," vol. 58, no. 1, pp. 348–362, Jan. 2020.
- [37] Z. Yue, Q. Zhao, J. Xie, L. Zhang, D. Meng, and K.-Y. K. Wong, "Blind image super-resolution with elaborate degradation modeling on noise and kernel," New Orleans, LA, Jun. 2022, pp. 2118–2128.
- [38] Y. Huang, E. Chouzenoux, and J.-C. Pesquet, "Unrolled variational bayesian algorithm for image blind deconvolution," vol. 32, pp. 430–445, 2023.
- [39] S. Gao and X. Zhuang, "Bayesian image super-resolution with deep modeling of image statistics," vol. 45, no. 2, pp. 1405–1423, Feb. 2023.
- [40] M. Zhang, B. Vozel, K. Chehdi, M. Uss, S. Abramov, and V. Lukin, "Blind estimation of blur in hyperspectral images," in *Image and Signal Processing for Remote Sensing XXIII*. Warsaw, Poland: Proc. SPIE 10427, Oct. 2017.
- [41] N. Wurst and J. Meola, "Impact of platform motion on hyperspectral imaging target detection and ground resolution distance," in *Algorithms and Technologies for Multispectral, Hyperspectral, and Ultraspectral Imagery XXIV*. Orlando, FL: Proc. SPIE 10644, May 2018.
- [42] H. Zhao, H. Shang, and G. Jia, "Simulation of remote sensing imaging motion blur based on image motion vector field," vol. 8, no. 1, Oct. 2014.
- [43] L. De Lathauwer, "Decompositions of a higher-order tensor in block terms—Part II: Definitions and uniqueness," *SIAM Journal on Matrix Analysis and Applications*, vol. 30, no. 3, pp. 1033–1066, 2008.
- [44] T. G. Kolda and B. W. Bader, "Tensor decompositions and applications," *SIAM Review*, vol. 51, no. 3, pp. 455–500, 2009.
- [45] G. H. Golub and C. F. Van Loan, *Matrix Computations*, 4th ed. Baltimore, MD: The Johns Hopkins University Press, 2013.
- [46] R. Dian, S. Li, L. Fang, T. Lu, and J. M. Bioucas-Dias, "Nonlocal sparse tensor factorization for semiblind hyperspectral and multispectral image fusion," vol. 50, no. 10, p. 4469, Oct. 2020.
- [47] Y. Chen, J. Zeng, W. He, X.-L. Zhao, and T.-Z. Huang, "Hyperspectral and multispectral image fusion using factor smoothed tensor ring decomposition," vol. 60, 2022.
- [48] X. Zhang, J. Zheng, D. Wang, G. Tang, Z. Zhou, and Z. Lin, "Structured sparsity optimization with non-convex surrogates of $\ell_{2,0}$ -norm: A unified algorithmic framework," vol. 45, no. 5, pp. 6386–6402, May 2023.
- [49] Y. Peng, D. Meng, Z. Xu, C. Gao, Y. Yang, and B. Zhang, "Decomposable nonlocal tensor dictionary learning for multispectral image denoising," Columbus, OH, Jun. 2014, pp. 2945–2956.
- [50] J. Xue, Y. Zhao, W. Liao, J. C.-W. Chan, and S. G. Kong, "Enhanced sparsity prior model for low-rank tensor completion," vol. 31, no. 11, pp. 4567–4581, Nov. 2020.
- [51] Y. Qiu, G. Zhou, Q. Zhao, and S. Xie, "Noisy tensor completion via low-rank tensor ring," to appear.
- [52] L. Chen, X. Jiang, X. Liu, and Z. Zhou, "Logarithmic norm regularized low-rank factorization for matrix and tensor completion," vol. 30, pp. 3434–3449, 2021.
- [53] Q. Xie, Q. Zhao, D. Meng, and Z. Xu, "Kronecker-basis-representation based tensor sparsity and its applications to tensor recovery," vol. 40, no. 8, pp. 1888–1902, Aug. 2017.
- [54] M. Yang, Q. Luo, W. Li, and M. Xiao, "3-D array image data completion by tensor decomposition and nonconvex regularization approach," vol. 70, pp. 4291–4304, 2022.
- [55] W. Chen, X. Gong, and N. Song, "Nonconvex robust low-rank tensor reconstruction via an empirical Bayes method," vol. 67, no. 22, pp. 5785–5797, Nov. 2019.
- [56] L. Zhang, L. Song, B. Du, and Y. Zhang, "Nonlocal low-rank tensor completion for visual data," *IEEE Transactions on Cybernetics*, vol. 51, no. 2, pp. 673–685, 2021.
- [57] J. Wright and Y. Ma, *High-Dimensional Data Analysis with Low-Dimensional Models*. Cambridge University Press, 2022.